THE JOURNAL OF BIOLOGICAL CHEMISTRY
Vol. 278, No. 19, Issue of May 9, pp. 17255–17262, 2003
Printed in U.S.A.

The Stress- and Inflammatory Cytokine-induced Ectodomain Shedding of Heparin-binding Epidermal Growth Factor-like Growth Factor Is Mediated by p38 MAPK, Distinct from the 12-*O*-Tetradecanoylphorbol-13-acetate- and Lysophosphatidic Acid-induced Signaling Cascades*

Received for publication, November 20, 2002, and in revised form, February 24, 2003
Published, JBC Papers in Press, February 28, 2003, DOI 10.1074/jbc.M211835200

Hisanori Takenobu‡, Ayano Yamazaki‡, Michinari Hirata‡, Toshiyuki Umata§¶, and Eisuke Mekada‡‖

From the ‡Department of Cell Biology, Research Institute for Microbial Diseases, Osaka University, Suita, Osaka 565-0871, Japan and the §Institute of Life Science, Kurume University, Kurume, Fukuoka 839-0861, Japan

Heparin-binding epidermal growth factor-like growth factor (HB-EGF) is a critical growth factor for a number of physiological and pathological processes. HB-EGF is synthesized as a membrane-anchored form (pro-HB-EGF), and pro-HB-EGF is cleaved at the cell surface to yield soluble HB-EGF by a mechanism called "ectodomain shedding." We show here that the ectodomain shedding of pro-HB-EGF in Vero cells is induced by various stress-inducing stimuli, including UV light, osmotic pressure, hyperoxidation, and translation inhibitors. The pro-inflammatory cytokine interleukin-1β also stimulated the ectodomain shedding of pro-HB-EGF. An inhibitor of p38 MAPK (SB203580) or the expression of a dominant-negative (dn) form of p38 MAPK inhibited the stress-induced ectodomain shedding of pro-HB-EGF, whereas an inhibitor of JNK (SP600125) or the expression of dnJNK1 did not. 12-*O*-Tetradecanoylphorbol-13-acetate (TPA) and lysophosphatidic acid (LPA) are also potent inducers of pro-HB-EGF shedding in Vero cells. Stress-induced pro-HB-EGF shedding was not inhibited by the inhibitors of TPA- or LPA-induced pro-HB-EGF shedding or by dn forms of molecules involved in the TPA- or LPA-induced pro-HB-EGF shedding pathway. Reciprocally, SB203580 or dnp38 MAPK did not inhibit TPA- or LPA-induced pro-HB-EGF shedding. These results indicate that stress-induced pro-HB-EGF shedding is mediated by p38 MAPK and that the signaling pathway induced by stress is distinct from the TPA- or LPA-induced pro-HB-EGF shedding pathway.

Heparin-binding epidermal growth factor (EGF)[1]-like growth factor (HB-EGF) (1), a member of the EGF family, binds to the EGF receptor (ErbB1) and the related receptor tyrosine kinase (ErbB4) and activates them (2). HB-EGF, especially the secreted form (sHB-EGF), is a potent mitogen and chemoattractant for a number of cell types, including vascular smooth muscle cells, fibroblasts, and keratinocytes (3). HB-EGF is implicated in a number of physiological and pathological processes in the body (4), which include wound healing (5, 6), kidney collecting duct morphogenesis (7), blastocyst implantation (8), cardiac hypertrophy (9–11), smooth muscle cell hyperplasia (12), pulmonary hypertension (13), and oncogenic transformation (14).

HB-EGF, synthesized as a membrane-anchored precursor protein (pro-HB-EGF) of 208 amino acids, is composed of a signal peptide, a heparin-binding domain, an EGF-like region, a juxtamembrane domain, a transmembrane segment, and a cytoplasmic tail (3). Pro-HB-EGF is cleaved at the cell surface within the juxtamembrane domain through a process called ectodomain shedding, which results in secretion of a soluble 75–86-amino acid growth factor (sHB-EGF) (15). Although the regulated process of pro-HB-EGF ectodomain shedding yields substantial sHB-EGF, a considerable amount remains uncleaved at the cell surface. In addition to being a precursor of sHB-EGF, pro-HB-EGF is a biologically active molecule, forming a complex with both CD9 (16) and integrin $\alpha_3\beta_1$ (17) to transduce biological signals to neighboring cells in a non-diffusible manner (18). In contrast to the mitogenic effect of sHB-EGF (4), pro-HB-EGF negatively regulates cell proliferation (19). These results suggest that strict control of pro-HB-EGF ectodomain shedding is critical for the proper regulation of the activity of this growth factor.

Pro-HB-EGF ectodomain shedding is induced by both physiological and pharmacological agonists such as 12-*O*-tetradecanoylphorbol-13-acetate (TPA). TPA, an activator of protein kinase C (PKC), potently induces the ectodomain shedding of pro-HB-EGF (15) and of other membrane proteins (20). In monkey kidney Vero cells, the presence of a constitutively active form of PKCδ results in the ectodomain shedding of pro-HB-EGF, and dominant-negative (dn) PKCδ suppresses TPA-induced shedding, suggesting that the PKCδ isoform contributes to the ectodomain shedding of pro-HB-EGF. PKCδ binds to the cytoplasmic domain of ADAM9/MDC9/meltrin-γ

* This work was supported by the Research for the Future Program of the Japan Society for the Promotion of Science and by grants-in-aid from the Ministry of Education, Culture, Sports, Science, and Technology (to E. M.). The costs of publication of this article were defrayed in part by the payment of page charges. This article must therefore be hereby marked "*advertisement*" in accordance with 18 U.S.C. Section 1734 solely to indicate this fact.

¶ Present address: Radioisotope Research Center, University of Occupational and Environmental Health, Kitakyushu 807-8555, Japan.

‖ To whom correspondence should be addressed. Tel.: 81-6-6879-8286; Fax: 81-6-6879-8289; E-mail: emekada@biken.osaka-u.ac.jp.

[1] The abbreviations used are: EGF, epidermal growth factor; HB-EGF, heparin-binding EGF-like growth factor; sHB-EGF, soluble HB-EGF; TPA, 12-*O*-tetradecanoylphorbol-13-acetate; PKC, protein kinase C; dn, dominant-negative; LPA, lysophosphatidic acid; MAPK, mitogen-activated protein kinase; MEK, MAPK/extracellular signal-regulated kinase kinase; MKK, MAPK kinase; IL, interleukin; TNF-α, tumor necrosis factor-α; GFP, green fluorescent protein; EGFP, enhanced GFP; JNK, c-Jun N-terminal kinase; SAPK, stress-activated protein kinase.

(21), a metalloprotease belonging to the ADAM (a disintegrin and metalloprotease) family (22). Overexpression of ADAM9 induces pro-HB-EGF shedding, which can be inhibited by the expression of the dnADAM9 mutant H347A,H351A in Vero-H cells. Thus, ADAM9 is thought to act downstream of PKCδ in the pro-HB-EGF shedding pathway (21), although the role of this protease in the direct cleavage of pro-HB-EGF remains unclear.

Lysophosphatidic acid (LPA) and other ligands of the seven-transmembrane G protein-coupled receptors also stimulate pro-HB-EGF shedding (23, 24). The activation of shedding by such ligands is crucial for the transactivation of the EGF receptor by G protein-coupled receptor ligands (23, 25, 26). In Vero cells, the Ras-Raf-MEK and Rac signaling pathways are activated in LPA-induced shedding (27). LPA-induced shedding is inhibited by dnHa-Ras, dnRac1, and the MEK inhibitor PD98059, but not by either dnPKCδ or dnADAM9. Conversely, although TPA-induced shedding is inhibited by dnPKCδ and dnADAM9, such shedding is not affected by dnHa-Ras, dnRac1, and the MEK inhibitor. These results indicate that two distinct signaling pathways function to regulate pro-HB-EGF ectodomain shedding, here designated the LPA- and TPA-induced pathways.

Pro-HB-EGF expression is enhanced in various tissues upon injury and inflammation (28–35). The induction of this cellular response under these conditions suggests that HB-EGF is involved in both physiological tissue repair, including processes such as wound healing, and pathological processes, including atherosclerosis, that follow from inappropriate inflammation. Cellular stress and inflammation may function as triggers of ectodomain shedding. It remains unclear, however, if inflammatory cytokines and stimuli inducing cellular stress responses can trigger pro-HB-EGF ectodomain shedding. We demonstrate here that various stress-inducing stimuli and inflammatory cytokines strongly induce ectodomain shedding, acting through a p38 MAPK-mediated pathway, distinct from both the TPA- and LPA-induced signaling pathways. Our results suggest that HB-EGF activity is regulated at the transcriptional level and by ectodomain shedding, which responds to stress and inflammation.

EXPERIMENTAL PROCEDURES

Reagents—TPA, Ro-31-8220, and anisomycin were purchased from Nacelle Tesque Co., Ltd. (Kyoto, Japan). LPA was obtained from Funakoshi Co., Ltd. (Tokyo, Japan). Recombinant human IL-1β, human TNF-α, and mouse IL-6 were acquired from PeproTech (Rocky Hill, NJ). PD98059 and SB203580 were purchased from Calbiochem. SP600125 was obtained from BIOMOL Research Labs Inc. (Plymouth Meeting, PA). H_2O_2 was acquired from Santoku Chemical Industries Co., Ltd. (Tokyo). KB-R8301 was obtained from Nippon Organon K. K. (Osaka, Japan).

Antibodies—The goat antibody specific for the C terminus of human pro-HB-EGF (C-18) was purchased from Santa Cruz Biotechnology (Santa Cruz, CA). Goat anti-HB-EGF neutralizing antibody was obtained from R&D Systems. A rabbit antiserum against the N terminus of human pro-HB-EGF (H6) was derived as described (36). Rabbit anti-mouse ADAM9 antibody was raised against a glutathione *S*-transferase fusion protein containing the mouse ADAM9 C-terminal region (amino acids 718–845). Horseradish peroxidase-conjugated goat anti-rabbit and unconjugated anti-FLAG (M2) monoclonal antibodies were purchased from Zymed Laboratories Inc. and Sigma, respectively. Horseradish peroxidase- and Cy3-conjugated donkey anti-goat antibodies were obtained from Chemicon International, Inc. (Temecula, CA).

Plasmids—pEGFP-c1, a plasmid encoding GFP, was purchased from Clontech. dnPKCδ (R144A, R145A, K376R) (37, 38) and the mouse dnADAM9 mutant H347A,H351A (21) have been described previously. The FLAG-tagged mouse ADAM9 mutant E348A was generated by site-directed PCR-based mutagenesis. FLAG-tagged dnRac1 (N17Rac1) has been described previously (27). FLAG-tagged dnp38 MAPK (T180A,Y182F) was kindly provided by H. Hatanaka and Y. Ishikawa (Institute of Protein Research, Osaka University). pCMV5-JNK1(APF), a plasmid encoding FLAG-tagged dnJNK1 (39), and a constitutively active form of MKK6 (EE-MKK6) (40) were kindly provided by R. J. Davis (University of Massachusetts Medical School) and Y. Gotoh (University of Tokyo), respectively.

Cell Culture and Transfection—Vero-H cells (15) were maintained in modified Eagle's medium with nonessential amino acids supplemented with 10% fetal calf serum. Transfections into Vero-H cells were performed using the calcium phosphate technique (41) unless otherwise stated.

Shedding Analysis by Western Blotting—Vero-H cells (5×10^5 cells/6-cm dish) were cultured for 6–12 h in serum-free modified Eagle's medium with nonessential amino acids and then treated with TPA (64 nM), LPA (20 μg/ml), IL-1β (4 ng/ml), anisomycin (10 μg/ml), sorbitol (0.4 M), or H_2O_2 (0.5 mM). When indicated, cells were also treated with either TNF-α (50 ng/ml) or IL-6 (20 ng/ml). For UV irradiation, Vero-H cells in 6-cm dishes in 3 ml of modified Eagle's medium with nonessential amino acids were exposed to 40 mJ/cm^2 UV radiation (254 nm) using a Spectrolinker (Spectronics Corp.) Following incubation for 30 min with stimuli, cells were collected and resuspended in 140 μl of lysis buffer (1% Nonidet P-40, 50 mM Tris-HCl, 0.1 M NaCl, 10 mM $MgCl_2$, 1 mM EDTA, 1 mM dithiothreitol, 0.2 mM phenylmethylsulfonyl fluoride, 20 μg/ml antipain, and 10 μg/ml chymostatin, pH 7.4). After 5 min on ice, the lysates were clarified by centrifugation at 15,000 rpm. Western blot analysis was performed using a goat antibody specific for the human pro-HB-EGF C terminus. The antibody was visualized with horseradish peroxidase-conjugated anti-goat IgG using ECL Plus (Amersham Biosciences). To detect sHB-EGF in the culture medium, sHB-EGF was trapped with heparin-Sepharose beads and then eluted with SDS gel sample buffer. The eluted materials were subjected to Western blot analysis and detected with rabbit anti-human HB-EGF antibody H6. The antibody was visualized with horseradish peroxidase-conjugated anti-rabbit IgG using ECL Plus.

Immunofluorescence Detection of the Shedding of the Pro-HB-EGF Ectodomain—Pro-HB-EGF was detected on cells using goat anti-HB-EGF neutralizing antibody and Cy3-conjugated anti-goat IgG as described (21). To detect the expression of transfected proteins, fixed cells were permeabilized with 0.1% Triton X-100 for 3 min and then stained with anti-FLAG antibody or the antibodies indicated, followed by fluorescein isothiocyanate-conjugated second antibody. To detect cells transfected with dnPKCδ or vector (pEF-BOS) alone as a control, EGFP (pEGFP-c1) was cotransfected. Images were captured with FISH Imager™ system (Carl Zeiss, Inc.). The percentage of pro-HB-EGF-positive cells was determined by counting the number of pro-HB-EGF-positive cells among the total cells concomitantly expressing the products of the transfected cDNA. Values were determined based on the results obtained in at least two independent transfections from at least 100 independent cells positive for either the transfected or marker proteins in each experiment. Scoring was performed in a completely blind manner.

RESULTS

Stimuli Inducing Various Stresses and IL-1β Lead to Pro-HB-EGF Shedding—Vero-H cells are stable Vero transfectants overexpressing human pro-HB-EGF (15). This cell line exhibits consistent responses to stimuli inducing pro-HB-EGF ectodomain shedding (21, 24, 27). Using Vero-H cells, we examined the effect of pro-inflammatory cytokines and stress-inducing stimuli on the induction of pro-HB-EGF ectodomain shedding. First, we examined the ectodomain shedding of pro-HB-EGF by immunofluorescence microscopy using an antibody specific for the pro-HB-EGF ectodomain. Vero-H cells were pretreated with the indicated stimuli and then cultured for 30 min. Cells were treated with anti-HB-EGF neutralizing antibody and then fixed and visualized using a secondary antibody. Pro-HB-EGF fluorescence at the cell surface disappeared following addition of either LPA (20 μg/ml) or TPA (64 nM) to the culture medium (Fig. 1A) (21, 24, 27). In addition, the pro-inflammatory cytokine IL-1β (4 μg/ml) also led to the disappearance of pro-HB-EGF surface immunofluorescence. Moreover, stimuli well known to induce a cellular stress response (42), such as translation inhibitors (anisomycin, 10 μg/ml) (43), exposure to UV light (40 mJ/cm^2), hypertonic osmotic pressure (sorbitol, 0.4 M), or oxidative stress (H_2O_2, 0.5 mM), also induced the disappearance of pro-HB-EGF immunofluorescence from the cell surface.

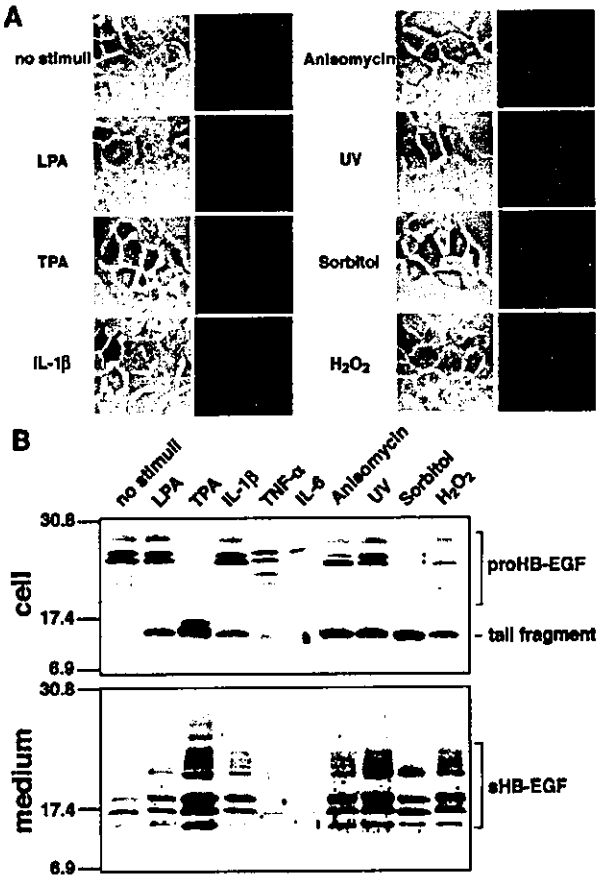

FIG. 1. **Stress- and inflammatory cytokine-induced ectodomain shedding of pro-HB-EGF.** Vero-H cells were treated with LPA (20 μg/ml), TPA (64 nM), IL-1β (4 ng/ml), TNF-α (50 ng/ml), IL-6 (20 ng/ml), anisomycin (10 μg/ml), UV light (40 mJ/cm^2), sorbitol (0.4 M), or H_2O_2 (0.5 mM) for 30 min, and then ectodomain shedding was detected by immunostaining of pro-HB-EGF and Western blot analysis. *A*, immunofluorescence detection of pro-HB-EGF at the cell surface. Cells were stained with anti-pro-HB-EGF neutralizing antibody, followed by Cy3-conjugated anti-goat IgG. The representative images for the samples treated with LPA, TPA, IL-1β, anisomycin, UV light, sorbitol, and H_2O_2 are shown. The *left panels* are phase-contrast images, whereas the *right panels* are immunofluorescence images. *B*, Western blot analysis. The *upper panel* illustrates full-length pro-HB-EGF and the tail fragment within cell lysates, detected using an antibody raised against the pro-HB-EGF C terminus. The *lower panel* shows sHB-EGF appearing in the culture medium, detected using an antibody raised against the pro-HB-EGF N terminus.

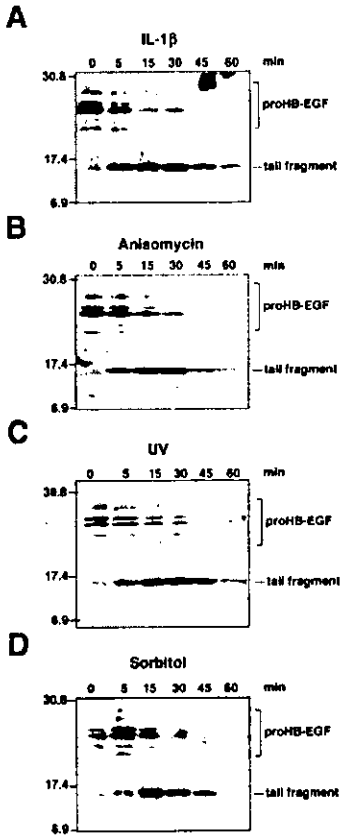

FIG. 2. **Time course of stress- and IL-1β-induced ectodomain shedding.** Vero-H cells were treated with 4 ng/ml IL-1β (*A*), 10 μg/ml anisomycin (*B*), 40 mJ/cm^2 UV light (*C*), or 0.4 M sorbitol (*D*). After the times indicated, the cells were harvested, and the cell lysates were analyzed by Western blotting with an antibody raised against the pro-HB-EGF C terminus.

Western blot analysis confirmed the ectodomain shedding of pro-HB-EGF in Vero-H cells (Fig. 1*B*). Immunoblot analysis of Vero-H cell lysates (*upper panel*) and the culture medium (*lower panel*) following incubation with the indicated stimuli detected the cytoplasmic domain of pro-HB-EGF and the shed soluble EGF-like domain, respectively. In cell lysates, bands ranging from 20 to 30 kDa correspond to pro-HB-EGF, whereas bands between 17.4 and 6.9 kDa are proteolytic fragments composed of the cytoplasmic and transmembrane domains of pro-HB-EGF (referred to as the "tail fragment"). Consistent with the appearance of the tail fragment, sHB-EGF appeared concurrently in the culture medium. These results indicate that IL-1β, anisomycin, UV light, and sorbitol, in addition to LPA and TPA, induce pro-HB-EGF cleavage to generate both the tail fragment in cell lysates and sHB-EGF in the culture medium. Although H_2O_2 generated the tail fragment in cell lysates and sHB-EGF in the culture medium, this stimulus also reduced the total pro-HB-EGF protein present through an unknown mechanism. Centrifuging as a mimic of shearing stress also induced pro-HB-EGF ectodomain shedding (data not shown). In contrast, the pro-inflammatory cytokines TNF-α and IL-6 did not affect shedding. Rather, these cytokines reduced the total pro-HB-EGF protein, although the reduced level varied depending on the experiments.

We also examined the time course of pro-HB-EGF shedding induced by IL-1β, anisomycin, UV light, and sorbitol. As the appearance of sHB-EGF in the culture medium correlated well with the appearance of the tail fragment in the cell lysate (Fig. 1*B*) (27), we utilized Western blot analysis only for the cell lysates to examine this event. As shown in Fig. 2, ectodomain shedding was observed following treatment with each of these stress stimuli at a time course similar to that observed for TPA-induced shedding (15, 21).

Stress-induced Pro-HB-EGF Shedding Involves p38 MAPK—Signals from pro-inflammatory cytokines and cellular responses to stress are generally mediated by SAPKs (42). Therefore, we hypothesized that stress-induced pro-HB-EGF shedding is mediated by a SAPK family kinase. We examined the activation of p38 MAPK and the various JNKs, major members of the SAPK family, following stress-inducing stimulation of Vero-H cells. After treatment with LPA, TPA, IL-1β, anisomycin, UV irradiation, or sorbitol, Vero-H cell lysates were analyzed by Western blotting with either anti-phospho-p38 MAPK or anti-phospho-JNK antibody to monitor kinase phosphorylation status. Phosphorylated p38 MAPK was strongly observed after treatment with anisomycin, UV light, or sorbitol, with moderate increases in phosphorylation follow-

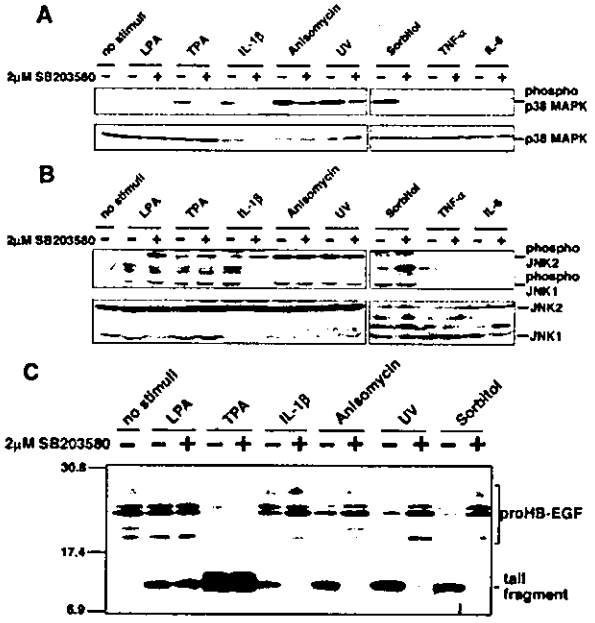

FIG. 3. **Effects of SB203580 on the activation of p38 MAPK and JNK1/2 or on pro-HB-EGF ectodomain shedding.** Serum-starved Vero-H cells were pretreated with or without 2 μM SB203580 for 1 h. Cells were then treated with IL-1β or stress-inducing or other stimuli for 30 min. Cell lysates were analyzed by Western blotting to detect activation of p38 MAPK and JNK1/2 and ectodomain shedding. *A*, activation level of p38 MAPK, detected with anti-phospho-p38 MAPK antibody (*upper panels*) and anti-p38 MAPK antibody (*lower panels*). *B*, activation level of JNK1/2, detected with anti-phospho-JNK1/2 antibody (*upper panels*) and anti-JNK1/2 antibody (*lower panels*). *C*, ectodomain shedding of pro-HB-EGF, detected by Western blotting using an antibody raised against the pro-HB-EGF C terminus.

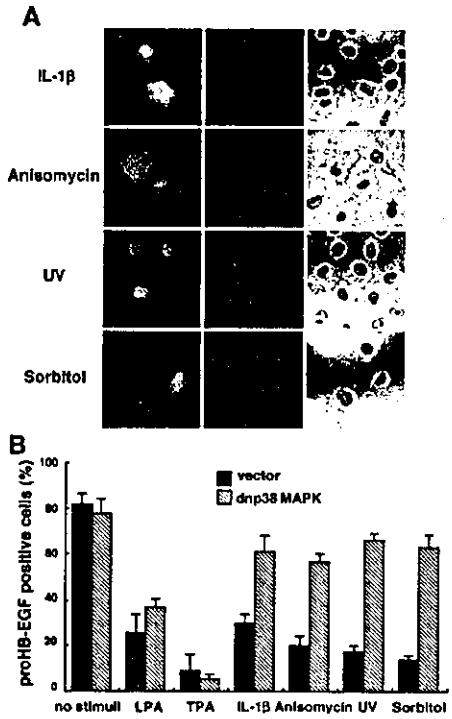

FIG. 4. **Inhibition of stress- and IL-1β-induced ectodomain shedding by dnp38 MAPK.** *A*, Vero-H cells were transfected with a plasmid encoding FLAG-tagged dnp38 MAPK (20 μg) or with vector (18 μg) plus EGFP (2 μg) as a control. After 48 h of transfection, the cells were incubated with LPA, TPA, IL-1β, anisomycin, UV light, or sorbitol and then double-stained with anti-HB-EGF antibody for the detection of the pro-HB-EGF ectodomain (*red*) and with anti-FLAG antibody for the detection of dnp38 MAPK expression (*green*). The *right panels* are phase-contrast images. Only the representative images of dnp38 MAPK-transfected cells are shown. *B*, shown is the percentage of pro-HB-EGF-positive cells among transfected cells, determined by immunofluorescence detection as shown in *A*. For vector-transfected cells, the percentage of pro-HB-EGF-positive cells among GFP-positive cells was determined.

ing treatment with either TPA or IL-1β. SB203580, an inhibitor of p38 MAPK (44), significantly reduced p38 MAPK activity at a concentration of 2 μM (Fig. 3*A*). JNK1/2 and p38 MAPK were activated by treatment with LPA, TPA, IL-1β, anisomycin, UV light, and sorbitol, although 2 μM SB203580 could not inhibit JNK1/2 phosphorylation (Fig. 3*B*). The results confirm that SB203580 specifically inhibits p38 MAPK activation. TNF-α and IL-6 could not activate either p38 MAPK (Fig. 3*A*) or JNK (Fig. 3*B*) in Vero-H cells, concurring with a lack of pro-HB-EGF cleavage (Fig. 1*B*).

We next inspected the SB203580 inhibition of pro-HB-EGF ectodomain shedding induction by IL-1β, anisomycin, UV light, or sorbitol to verify the involvement of p38 MAPK. 2 μM SB203580 drastically inhibited the stress-induced shedding caused by IL-1β, anisomycin, UV light, or sorbitol (Fig. 3*C*), whereas TPA- and LPA-induced shedding was not affected. Even concentrations of SB203580 in excess of 10 μM could not inhibit TPA- and LPA-induced shedding (data not shown). These results suggest that pro-HB-EGF ectodomain shedding induced by IL-1β, anisomycin, UV light, or sorbitol requires p38 MAPK activation.

We examined the requirement for p38 MAPK in stress-induced pro-HB-EGF shedding using dnp38 MAPK. Following the transfection of FLAG-tagged dnp38 MAPK, cells were treated with various stimuli and then double-stained for pro-HB-EGF and dnp38 MAPK. Although treatment with IL-1β, anisomycin, UV light, or sorbitol enhanced pro-HB-EGF shedding in vector-transfected cells (Fig. 4*B*), shedding was inhibited in FLAG-positive cells expressing dnp38 MAPK (Fig. 4, *A* and *B*). We confirmed that LPA- and TPA-induced pro-HB-EGF ectodomain shedding was not inhibited by dnp38 MAPK (Fig. 4*B*). MKK6 is a specific activator of p38 MAPK (45). Consistent with the role of the p38 MAPK pathway in shedding, transfection of a constitutively active form of MKK6 resulted in pro-HB-EGF ectodomain shedding in the absence of stress-inducing stimuli in a dose-dependent manner (Fig. 5). These results indicate that p38 MAPK activation is required for stress-induced pro-HB-EGF shedding in Vero-H cells.

SB203580 (2 μM) reduced the activity of p38 MAPK, but not that of JNK1/2, as shown in Fig. 3 (*A* and *B*). At the same concentration, SB203580 inhibited stress-induced shedding, suggesting that JNK is not involved in stress-induced shedding in Vero-H cells. To examine the involvement of JNK in stress-induced shedding directly, we tested whether SP600125, an inhibitor of JNK (46), abrogates stress-induced pro-HB-EGF shedding in Vero-H cells. SP600125 (5 μM) significantly reduced JNK1/2 phosphorylation caused by TPA, IL-1β, anisomycin, and sorbitol treatment (Fig. 6*A*), whereas the same concentration of SP600125 could not inhibit p38 MAPK phosphorylation caused by IL-1β, anisomycin, and sorbitol treatment (Fig. 6*B*). Based on these results, we tested whether SP600125 inhibits stress-induced ectodomain shedding in Vero-H cells. SP600125 (5 μM) did not inhibit pro-HB-EGF ectodomain shedding induced by any stimulus (Fig. 6*C*). In UV light-irradiated cells, JNK1/2 phosphorylation was strong and was not significantly reduced with 5 μM SP600125. SP600125 (20 μM) inhibited JNK1/2 phosphorylation caused by UV light, but SP600125 scarcely inhibited UV light-induced shedding even at this concentration.

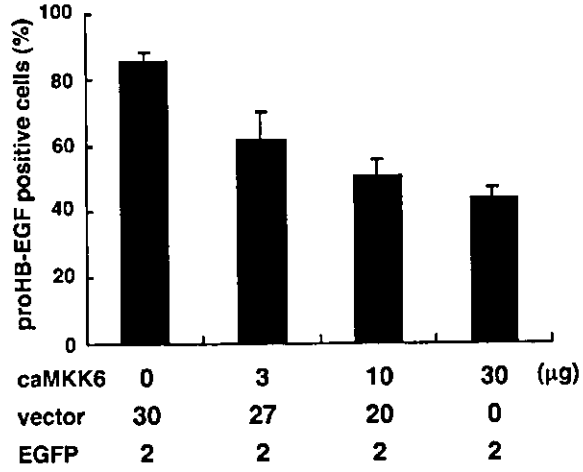

FIG. 5. **Enhanced ectodomain shedding by a constitutively active form of MKK6.** Vero-H cells were transfected with a plasmid encoding constitutively active (*ca*) MKK6 by electroporation (Bio-Rad, Gene Pulser) according to the manufacturer's instruction. The empty vector (pEF-BOS) and a plasmid encoding EGFP were also cotransfected at the amounts indicated. The percentage of pro-HB-EGF-positive cells among GFP-positive cells was determined.

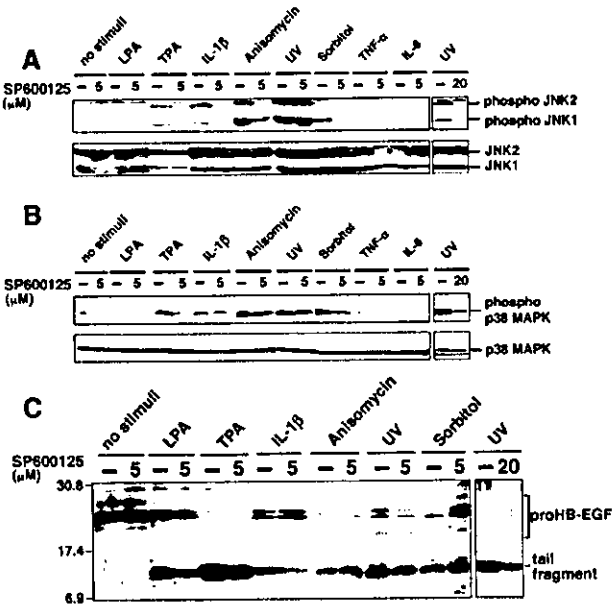

FIG. 6. **Effects of the JNK inhibitor SP600125 on stress-induced ectodomain shedding.** Serum-starved Vero-H cells were pretreated with or without SP600125 at the indicated concentrations for 1 h and then treated with IL-1β or stress-inducing or other stimuli for 30 min. Cell lysates were analyzed by Western blotting to detect activation of JNK1/2 and p38 MAPK and ectodomain shedding. *A* and *B*, activation levels of JNK1/2 and p38 MAPK, respectively. *C*, ectodomain shedding of pro-HB-EGF.

In addition to the JNK inhibitor, we used dnJNK1 to examine the involvement of the JNK pathway in stress-induced pro-HB-EGF shedding. Following the transfection of FLAG-tagged dnJNK1, cells were treated with various stimuli as Fig. 4*B* and then double-stained for pro-HB-EGF and dnJNK1. Pro-HB-EGF ectodomain shedding induced by each stimulus was not inhibited in FLAG-positive cells expressing dnJNK1 (Fig. 7). From these results, we conclude that the JNK pathway is not involved in stress-induced pro-HB-EGF ectodomain shedding in Vero-H cells.

p38 MAPK-mediated Shedding Cascades Are Independent of the Other Shedding Cascades—Using Vero-H cells, we demonstrated that the LPA-induced shedding cascade involves the Ras-Raf-MEK and small GTPase Rac pathways, whereas TPA-induced pro-HB-EGF shedding involves PKCδ and ADAM9. IL-1β, anisomycin, and additional stresses induce shedding through a pathway involving the activation of p38 MAPK. We next analyzed the connection of the p38 MAPK-mediated pathway with either the LPA- or TPA-induced pathway. We tested the effect of the MEK inhibitor PD98059 (47) and the PKC inhibitor Ro-31-8220 (48) on p38 MAPK-mediated pro-HB-EGF ectodomain shedding. PD98059 inhibited LPA-induced, but not TPA-induced, shedding (Fig. 8*A*), whereas Ro-31-8220 inhibited TPA-induced, but not LPA-induced, shedding (Fig. 8*B*), confirming previous results (27). p38 MAPK-mediated stress-induced shedding was not inhibited by either PD98059 or Ro-31-8220. We also transfected dnPKCδ or dnRac1. Neither dnPKCδ nor dnRac1 inhibited p38 MAPK-mediated shedding, with the exception of partial inhibition observed for sorbitol-induced shedding by dnRac1 (Fig. 9). These data indicate that the stress-induced shedding cascade mediated by p38 MAPK activation functions independently of the LPA- and TPA-induced shedding cascades.

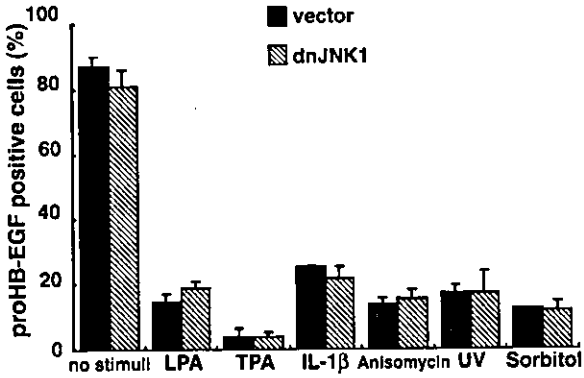

FIG. 7. **Effects of dnJNK1 on stress-induced ectodomain shedding.** Vero-H cells were transfected with a plasmid encoding FLAG-tagged dnJNK1 (20 μg) or with vector (pEF-BOS; 18 μg) plus EGFP (2 μg). After 48 h of transfection, the cells were incubated with LPA, TPA, IL-1β, anisomycin, UV light, or sorbitol and then stained with anti-HB-EGF antibody for the detection of the pro-HB-EGF ectodomain. The expression of dnJNK1 was detected by anti-FLAG antibody. The percentage of pro-HB-EGF-positive cells among FLAG-positive cells was determined. For cells transfected with the empty vector, the percentage of pro-HB-EGF-positive cells among GFP-positive cells was determined.

Metalloproteases Are Involved in Stress-induced Shedding—Metalloprotease inhibitors inhibit both TPA- and LPA-induced pro-HB-EGF shedding. We treated cells with a hydroxamic acid-based metalloprotease inhibitor, KB-R8301, to examine the role of metalloproteases in stress-induced shedding. KB-R8301 (10 μM) inhibited the pro-HB-EGF shedding induced by IL-1β, anisomycin, UV light, H_2O_2, and sorbitol (Fig. 10*A*), indicating that metalloproteases are required for p38 MAPK-mediated pro-HB-EGF shedding as well.

ADAM family metalloproteases are involved in the ectodomain shedding of a variety of proteins such as TNF-α and Delta (49, 50). ADAM9 is known to be involved in TPA-induced pro-HB-EGF shedding in Vero-H cells (21). To examine the role of ADAM9 in p38 MAPK-mediated shedding, we examined the effect of overexpression of dnADAM9 on shedding. Two ADAM9 mutants were used, one carrying the modification of the conserved histidine residues in the catalytic domain to alanines (H347A,H351A) and the other carrying a modification of the conserved glutamic acid in the catalytic domain to alanine (E348A). We investigated the influence of these mutants on stress- and IL-1β-induced shedding. Both mutants inhibited

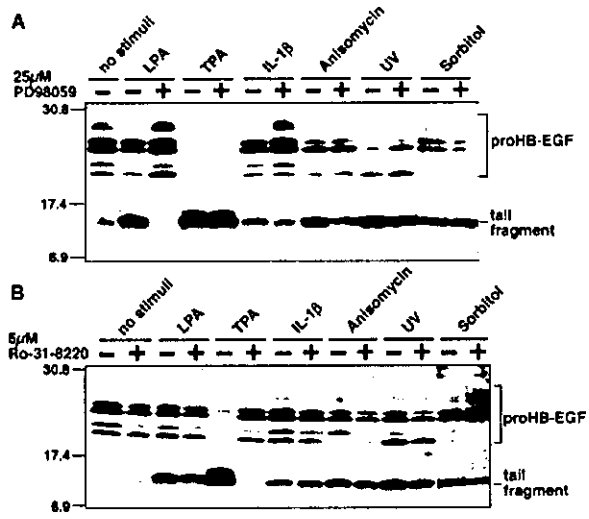

FIG. 8. **Effects of the MEK inhibitor PD98059 and the PKC inhibitor Ro-31-8220 on the ectodomain shedding of pro-HB-EGF.** Serum-starved Vero-H cells were pretreated with 25 μM PD98059 (*A*) or 5 μM Ro-31-8220 (*B*) for 1 h. As a control, 0.1% Me_2SO, the solvent of these inhibitors, was added. The cells were treated with each stimulus for 30 min. Ectodomain shedding was detected by Western blot analysis of cell lysates using an antibody raised against the pro-HB-EGF C terminus.

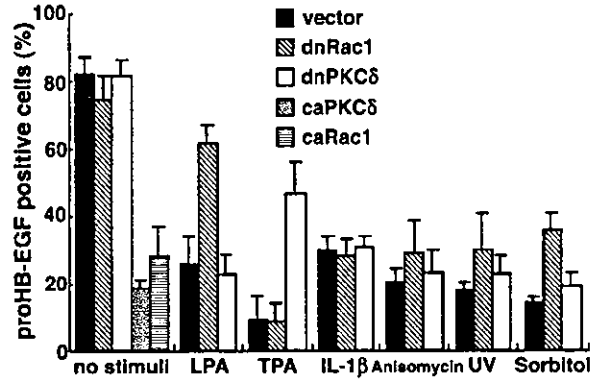

FIG. 9. **Effects of dnRac1 and dnPKCδ on the ectodomain shedding of pro-HB-EGF.** Vero-H cells were transfected with plasmids encoding FLAG-tagged dnRac1 (20 μg) and dnPKCδ (18 μg) plus EGFP (2 μg) or with vector (18 μg) plus EGFP (2 μg) as a control. After 48 h of transfection, the cells were incubated with LPA, TPA, IL-1β, anisomycin, UV light, or sorbitol and then stained with anti-HB-EGF antibody for the detection of the pro-HB-EGF ectodomain. The expression of dnRac1 was detected by anti-FLAG antibody. The percentage of pro-HB-EGF-positive cells among FLAG-positive cells was determined. For cells transfected with either dnPKCδ or the empty vector, the percentage of pro-HB-EGF-positive cells among GFP-positive cells was determined. *ca*, constitutively active.

TPA-induced shedding, but did not affect LPA-, stress-, and IL-1β-induced shedding (Fig. 10*B*). These results indicate that ADAM9 is not required for stress- and IL-1β-induced pro-HB-EGF shedding in Vero-H cells.

DISCUSSION

HB-EGF contributes to tissue repair processes acting in response to various injuries (5, 6, 30, 51). HB-EGF also participates in pathological processes, including smooth muscle cell hyperplasia (12), restenosis following balloon injury (52), and cardiac hypertrophy (9–11). Ectodomain shedding is critical for the biological activity of this growth factor (53). In addition to regulation of growth factor activity, pro-HB-EGF ectodomain shedding contributes to the transactivation of the EGF receptor

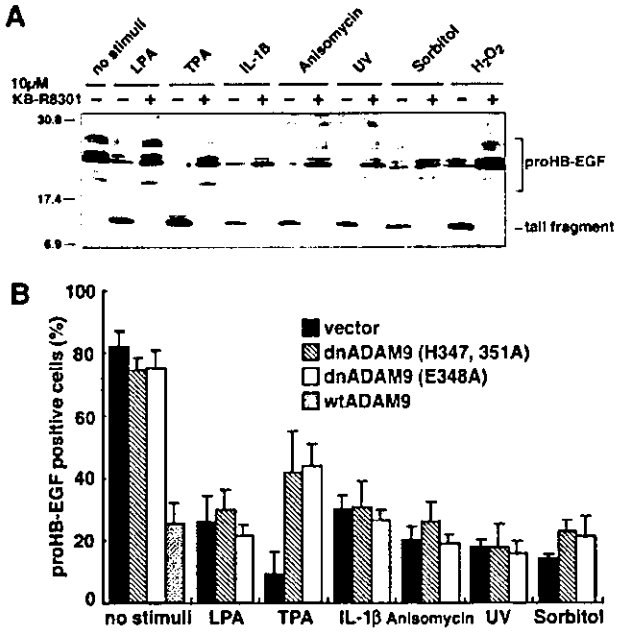

FIG. 10. **Inhibition of stress- and IL-1β-induced pro-HB-EGF shedding by the metalloprotease inhibitor KB-R8301, but not dnADAM9.** *A*, effect of the metalloprotease inhibitor KB-R8301. Vero-H cells were pretreated with 10 μM KB-R8301 or 0.1% Me_2SO for 1 h and then treated with each stimulus for 30 min. Ectodomain shedding was detected by Western blot analysis of cell lysates using an antibody raised against the pro-HB-EGF C terminus. *B*, effect of dnADAM9. Vero-H cells were transfected with plasmids encoding the dominant-negative mutants H347A,H351A (20 μg) and E348A (20 μg) or with vector alone (18 μg) plus EGFP (2 μg) as a control. After 48 h of transfection, cells were incubated with LPA, TPA, IL-1β, UV light, or sorbitol and then double-stained with either anti-HB-EGF or anti-ADAM9 antibody. The percentage of pro-HB-EGF-positive cells among ADAM9-positive cells was determined. *wt*, wild-type.

following ligation by G protein-coupled receptors and other ligands (23). Recent studies suggest that pro-HB-EGF ectodomain shedding and transactivation are involved in the pathological processes of cardiac hypertrophy and pulmonary hypertension (9, 13). Although a function for HB-EGF in physiological and pathological processes has been increasingly reported, information about shedding-inducing stimuli and the downstream signaling processes involved is limited (54). Two distinct signaling pathways contribute to pro-HB-EGF shedding in Vero-H cells, the TPA-induced PKCδ- and ADAM9-mediated pathway and the LPA-induced MEK- and Rac-mediated pathway. Using Vero-H cells, we determined that various stress-inducing and inflammatory stimuli also trigger ectodomain shedding in a p38 MAPK-mediated manner. As this cascade does not require the activation of MEK, Rac, PKCδ, or ADAM9, it appears to function independently of the TPA- and LPA-induced pathways. Thus, the p38 MAPK-mediated pathway is a third signal cascade that can induce pro-HB-EGF shedding in these cells.

Stress-induced ectodomain shedding is not specific to pro-HB-EGF. Osmotic stress induces L-selectin shedding in neutrophils (55). UV light and osmotic pressure promote the shedding of pro-transforming growth factor-α and proneuregulin in Chinese hamster ovary cells (56). Although stress activates both p38 MAPK and JNK, this and previous studies (55–57) suggest that p38 MAPK, rather than JNK, is the primary contributor to the stress-induced ectodomain shedding of a number of membrane proteins. Inflammatory cytokines, including TNF-α, IL-1β, and IL-6, also stimulate membrane protein shedding (58–60). In Vero-H cells, however, neither

ectodomain shedding nor p38 MAPK activation was observed following treatment with either TNF-α or IL-6 (Figs. 1*B* and 3*A*). Although it is possible that Vero-H cells do not bear the receptors ligating TNF-α and IL-6, it appears that signaling pathways induced by TNF-α and IL-6 do not contribute to pro-HB-EGF shedding.

We have demonstrated that stress- and IL-1β-induced shedding requires protease(s) abrogated by metalloprotease inhibitors. This result is in agreement with data obtained for TPA- and LPA-induced shedding and for additional shedding cascades of transmembrane molecules (61). Therefore, a metalloprotease such as matrix metalloprotease or ADAM that works in close proximity to the membrane may participate in pro-HB-EGF shedding. The ADAM family metalloproteases contains a conserved sequence (HEXXH) that is a putative zinc-binding motif within the catalytic domain. We previously constructed a mutant form of ADAM9 (H347A,H351A, in which the conserved histidines are replaced with alanines) that was found to inhibit TPA-induced pro-HB-EGF shedding (21). Thus, ADAM9 is involved in pro-HB-EGF shedding induced by treatment of Vero-H cells with TPA. In this study, we constructed another dnADAM9 mutant (E348A) to examine its effect on TPA-induced pro-HB-EGF shedding. As E348A exhibited a subcellular localization similar to that of native ADAM9 when expressed in Vero-H cells, E348A may be a more suitable dnADAM9 mutant than the H347A,H351A mutant, which exhibited an altered localization pattern. Both dominant-negative mutants inhibited TPA-induced shedding, confirming the role of ADAM9 in TPA-induced shedding. Neither H347A, H351A nor E348A inhibited LPA-, stress-, or IL-1β-induced pro-HB-EGF shedding in Vero-H cells. From these results, we conclude that ADAM9 does not participate in LPA-, stress-, or IL-1β-induced pro-HB-EGF shedding.

Recent studies suggest that, in addition to ADAM9, ADAM10/Kuzbanian (13, 62), ADAM12/meltrin-α (9), and ADAM17/TACE (TNF-α converting enzyme) (63) function in pro-HB-EGF shedding in various cell systems. We therefore constructed putative dnADAM10, dnADAM12, and dnADAM17 mutants by substituting the conserved glutamic acid within the catalytic domain with an alanine (Glu mutants). These mutants were tested for their ability to inhibit stress- and IL-1β-induced shedding in Vero-H cells. They did not prevent stress- and IL-1β-induced pro-HB-EGF shedding in Vero-H cells.[2] Although we have not confirmed the loss of catalytic activity by these constructed Glu mutants, these results suggest that ADAM10, ADAM12, and ADAM17 are not sheddases for stress- and IL-1β-induced pro-HB-EGF shedding in Vero-H cells. Thus, the protease responsible for p38 MAPK-mediated pro-HB-EGF shedding in Vero-H cells remained to be identified.

What is the biological significance of stress-induced pro-HB-EGF shedding? A number of reports indicate that the transcription of pro-HB-EGF is up-regulated in response to oxidative, ischemic, osmotic, and mechanical stresses (29–34). The inflammatory cytokines IL-1β and TNF-α also markedly increase pro-HB-EGF gene expression (35). The release of sHB-EGF from the membrane by ectodomain shedding is a prerequisite for the mitogenic activity as a paracrine and autocrine growth factor. Therefore, stress and inflammatory cytokines may also induce pro-HB-EGF shedding in addition to their transcriptional up-regulation. In response to stress and inflammation, HB-EGF activity may be regulated at both the transcriptional and ectodomain shedding levels. Considering the role of HB-EGF in tissue repair, the rapid release of sHB-EGF following stress-inducing stimuli may facilitate the repair of wounded tissues. These results also suggest that excess release of sHB-EGF by continual exposure of tissues to stress and inflammation may result in the pathological hyperplasia of cells such as smooth muscle and cardiac cells.

[2] A. Yamazaki and E. Mekada, unpublished data.

REFERENCES

1. Higashiyama, S., Abraham, J. A., Miller, J., Fiddes, J. C., and Klagsbrun, M. (1991) *Science* **251**, 936–939
2. Elenius, K., Paul, S., Allison, G., Sun, J., and Klagsbrun, M. (1997) *EMBO J.* **16**, 1268–1278
3. Higashiyama, S., Lau, K., Besner, G. E., Abraham, J. A., and Klagsbrun, M. (1992) *J. Biol. Chem.* **267**, 6205–6212
4. Raab, G., and Klagsbrun, M. (1997) *Biochim. Biophys. Acta* **1333**, F179–F199
5. Marikovsky, M., Breuing, K., Liu, P. Y., Eriksson, E., Higashiyama, S., Farber, P., Abraham, J., and Klagsbrun, M. (1993) *Proc. Natl. Acad. Sci. U. S. A.* **90**, 3889–3893
6. Tokumaru, S., Higashiyama, S., Endo, T., Nakagawa, T., Miyagawa, J. I., Yamamori, K., Hanakawa, Y., Ohmoto, H., Yoshino, K., Shirakata, Y., Matsuzawa, Y., Hashimoto, K., and Taniguchi, N. (2000) *J. Cell Biol.* **151**, 209–220
7. Takemura, T., Hino, S., Kuwajima, H., Yanagida, H., Okada, M., Nagata, M., Sasaki, S., Barasch, J., Harris, R. C., and Yoshioka, K. (2001) *J. Am. Soc. Nephrol.* **12**, 964–972
8. Das, S. K., Wang, X. N., Paria, B. C., Damm, D., Abraham, J. A., Klagsbrun, M., Andrews, G. K., and Dey, S. K. (1994) *Development* **120**, 1071–1083
9. Asakura, M., Kitakaze, M., Takashima, S., Liao, Y., Ishikura, F., Yoshinaka, T., Ohmoto, H., Node, K., Yoshino, K., Ishiguro, H., Asanuma, H., Sanada, S., Matsumura, Y., Takeda, H., Beppu, S., Tada, M., Hori, M., and Higashiyama, S. (2002) *Nat. Med.* **8**, 35–40
10. Fujino, T., Hasebe, N., Fujita, M., Takeuchi, K., Kawabe, J., Tobise, K., Higashiyama, S., Taniguchi, N., and Kikuchi, K. (1998) *Cardiovasc. Res.* **38**, 365–374
11. Perrella, M. A., Maki, T., Prasad, S., Pimental, D., Singh, K., Takahashi, N., Yoshizumi, M., Alali, A., Higashiyama, S., and Kelly, R. A. (1994) *J. Biol. Chem.* **269**, 27045–27050
12. Miyagawa, J., Higashiyama, S., Kawata, S., Inui, Y., Tamura, S., Yamamoto, K., Nishida, M., Nakamura, T., Yamashita, S., Matsuzawa, Y., and Taniguchi, N. (1995) *J. Clin. Invest.* **95**, 404–411
13. Lemjabbar, H., and Basbaum, C. (2002) *Nat. Med.* **8**, 41–46
14. Fu, S., Bottoli, I., Goller, M., and Vogt, P. K. (1999) *Proc. Natl. Acad. Sci. U. S. A.* **96**, 5716–5721
15. Goishi, K., Higashiyama, S., Klagsbrun, M., Nakano, N., Umata, T., Ishikawa, M., Mekada, E., and Taniguchi, N. (1995) *Mol. Biol. Cell* **6**, 967–980
16. Mitamura, T., Iwamoto, R., Umata, T., Yomo, T., Urabe, I., Tsuneoka, M., and Mekada, E. (1992) *J. Cell Biol.* **118**, 1389–1399
17. Nakamura, K., Iwamoto, R., and Mekada, E. (1995) *J. Cell Biol.* **129**, 1691–1705
18. Higashiyama, S., Iwamoto, R., Goishi, K., Raab, G., Taniguchi, N., Klagsbrun, M., and Mekada, E. (1995) *J. Cell Biol.* **128**, 929–938
19. Iwamoto, R., Handa, K., and Mekada, E. (1999) *J. Biol. Chem.* **274**, 25906–25912
20. Arribas, J., Coodly, L., Vollmer, P., Kishimoto, T. K., Rose-John, S., and Massagué, J. (1996) *J. Biol. Chem.* **271**, 11376–11382
21. Izumi, Y., Hirata, M., Hasuwa, H., Iwamoto, R., Umata, T., Miyado, K., Tamai, Y., Kurisaki, T., Sehara-Fujisawa, A., Ohno, S., and Mekada, E. (1998) *EMBO J.* **17**, 7260–7272
22. Weskamp, G., Kratzschmar, J., Reid, M. S., and Blobel, C. P. (1996) *J. Cell Biol.* **132**, 717–726
23. Prenzel, N., Zwick, E., Daub, H., Leserer, M., Abraham, R., Wallasch, C., and Ullrich, A. (1999) *Nature* **402**, 884–888
24. Hirata, M., Umata, T., Takahashi, T., Ohnuma, M., Miura, Y., Iwamoto, R., and Mekada, E. (2001) *Biochem. Biophys. Res. Commun.* **283**, 915–922
25. Eguchi, S., Dempsey, P. J., Frank, G. D., Motley, E. D., and Inagami, T. (2001) *J. Biol. Chem.* **276**, 7957–7962
26. Fujiyama, S., Matsubara, H., Nozawa, Y., Maruyama, K., Mori, Y., Tsutsumi, Y., Masaki, H., Uchiyama, Y., Koyama, Y., Nose, A., Iba, O., Tateishi, E., Ogata, N., Jyo, N., Higashiyama, S., and Iwasaka, T. (2001) *Circ. Res.* **88**, 22–29
27. Umata, T., Hirata, M., Takahashi, T., Ryu, F., Shida, S., Takahashi, Y., Tsuneoka, M., Miura, Y., Masuda, M., Horiguchi, Y., and Mekada, E. (2001) *J. Biol. Chem.* **276**, 30475–30482
28. Blotnick, S., Peoples, G. E., Freeman, M. R., Eberlein, T. J., and Klagsbrun, M. (1994) *Proc. Natl. Acad. Sci. U. S. A.* **91**, 2890–2894
29. Koh, Y. H., Che, W., Higashiyama, S., Takahashi, M., Miyamoto, Y., Suzuki, K., and Taniguchi, N. (2001) *J. Biochem. (Tokyo)* **130**, 351–358
30. Fang, L., Li, G., Liu, G., Lee, S. W., and Aaronson, S. A. (2001) *EMBO J.* **20**, 1931–1939
31. Miyazaki, Y., Hiraoka, S., Tsutsui, S., Kitamura, S., Shinomura, Y., and Matsuzawa, Y. (2001) *Gastroenterology* **120**, 108–116
32. Sakai, M., Tsukada, T., and Harris, R. C. (2001) *Exp. Nephrol.* **9**, 28–39
33. Nguyen, H. T., Adam, R. M., Bride, S. H., Park, J. M., Peters, C. A., and Freeman, M. R. (2000) *Am. J. Physiol.* **279**, C1155–C1167
34. Morita, T., Yoshizumi, M., Kurihara, H., Maemura, K., Nagai, R., and Yazaki, Y. (1993) *Biochem. Biophys. Res. Commun.* **197**, 256–262
35. Yoshizumi, M., Kourembanas, S., Temizer, D. H., Cambria, R. P., Quertermous, T., and Lee, M. E. (1992) *J. Biol. Chem.* **267**, 9467–9469
36. Iwamoto, R., Higashiyama, S., Mitamura, T., Taniguchi, N., Klagsbrun, M., and Mekada, E. (1994) *EMBO J.* **13**, 2322–2330
37. Hirai, S., Izumi, Y., Higa, K., Kaibuchi, K., Mizuno, K., Osada, S., Suzuki, K., and Ohno, S. (1994) *EMBO J.* **13**, 2331–2340

38. Ohno, S., Mizuno, K., Adachi, Y., Hata, A., Akita, Y., Akimoto, K., Osada, S., Hirai, S., and Suzuki, K. (1994) *J. Biol. Chem.* **269,** 17495–17501
39. Derijard, B., Hibi, M., Wu, I. H., Barrett, T., Su, B., Deng, T., Karin, M., and Davis, R. J. (1994) *Cell* **76,** 1025–1037
40. Fujishiro, M., Gotoh, Y., Katagiri, H., Sakoda, H., Ogihara, T., Anai, M., Onishi, Y., Ono, H., Funaki, M., Inukai, K., Fukushima, Y., Kikuchi, M., Oka, Y., and Asano T. (2001) *J. Biol. Chem.* **276,** 19800–19806
41. Chen, C., and Okayama, H. (1987) *Mol. Cell. Biol.* **7,** 2745–2752
42. Kyriakis, J. M., and Avruch, J. (2001) *Physiol. Rev.* **81,** 807–869
43. Cano, E., Hazzalin, C. A., and Mahadevan, L. C. (1994) *Mol. Cell. Biol.* **14,** 7352–7362
44. Lee, J. C., Laydon, J. T., McDonnell, P. C., Gallagher, T. F., Kumar, S., Green, D., McNulty, D., Blumenthal, M. J., Heys, J. R., Landvatter, S. W., Strickler, J. E., McLaughlin, M. M., Siemens, I. R., Fisher, S. M., Livi, G. P., White, J. R., Adams, J. L., and Young, P. R. (1994) *Nature* **372,** 739–746
45. Han, J., Lee, J. D., Jiang, Y., Li, Z., Feng, L., and Ulevitch, R. J. (1996) *J. Biol. Chem.* **271,** 2886–2891
46. Bennett, B. L., Sasaki, D. T., Murray, B. W., O'Leary, E. C., Sakata, S. T., Xu, W., Leisten, J. C., Motiwala, A., Pierce, S., Satoh, Y., Bhagwat, S. S., Manning, A. M., and Anderson, D. W. (2001) *Proc. Natl. Acad. Sci. U. S. A.* **98,** 13681–13686
47. Dudley, D. T., Pang, L., Decker, S. J., Bridges, A. J., and Saltiel, A. R. (1995) *Proc. Natl. Acad. Sci. U. S. A.* **92,** 7686–7689
48. Bradshaw, D., Hill, C. H., Nixon, J. S., and Wilkinson, S. E. (1993) *Agent Actions* **38,** 135–147
49. Blobel, C. P. (2000) *Curr. Opin. Cell Biol.* **12,** 606–612
50. Black, R. A., and White, J. M. (1998) *Curr. Opin. Cell Biol.* **10,** 654–659
51. Michalsky, M. P., Kuhn, A., Mehta, V., and Besner, G. E. (2001) *J. Pediatr. Surg.* **36,** 1130–1135
52. Igura, T., Kawata, S., Miyagawa, J., Inui, Y., Tamura, S., Fukuda, K., Isozaki, K., Yamamori, K., Taniguchi, N., Higashiyama, S., and Matsuzawa, Y. (1996) *Arterioscler. Thromb. Vasc. Biol.* **16,** 1524–1531
53. Iwamoto, R., and Mekada, E. (2000) *Cytokine Growth Factor Rev.* **11,** 335–344
54. Gechtman, Z., Alonso, J. L., Raab, G., Ingber, D. E., and Klagsbrun, M. (1999) *J. Biol. Chem.* **274,** 28828–28835
55. Rizoli, S. B., Rotstein, O. D., and Kapus, A. (1999) *J. Biol. Chem.* **274,** 22072–22080
56. Montero, J. C., Yuste, L., Diaz-Rodriguez, E., Esparis-Ogando, A., and Pandiella, A. (2002) *Biochem. J.* **363,** 211–221
57. Fan, H., and Derynck, R. (1999) *EMBO J.* **18,** 6962–6972
58. Franzke, C. W., Tasanen, K., Schacke, H., Zhou, Z., Tryggvason, K., Mauch, C., Zigrino, P., Sunnarborg, S., Lee, D. C., Fahrenholz, F., and Bruckner-Tuderman, L. (2002) *EMBO J.* **21,** 5026–5035
59. Levine, S. J., Logun, C., Chopra, D. P., Rhim, J. S., and Shelhamer, J. H. (1996) *Am. J. Respir. Cell Mol. Biol.* **14,** 254–261
60. Yabkowitz, R., Meyer, S., Black, T., Elliott, G., Merewether, L. A., and Yamane, H. K. (1999) *Blood* **93,** 1969–1979
61. Hooper, N. M., Karran, E. H., and Turner, A. J. (1997) *Biochem. J.* **321,** 265–279
62. Yan, Y., Shirakabe, K., and Werb, Z. (2002) *J. Cell Biol.* **158,** 221–226
63. Sunnarborg, S. W., Hinkle, C. L., Stevenson, M., Russell, W. E., Raska, C. S., Peschon, J. J., Castner, B. J., Gerhart, M. J., Paxton, R. J., Black, R. A., and Lee, D. C. (2002) *J. Biol. Chem.* **277,** 12838–12845

Report

Mice with defects in HB-EGF ectodomain shedding show severe developmental abnormalities

Satoru Yamazaki,[1] Ryo Iwamoto,[1] Kazuko Saeki,[2] Masanori Asakura,[3] Seiji Takashima,[3] Ayano Yamazaki,[1] Rina Kimura,[1] Hiroto Mizushima,[1] Hiroki Moribe,[1] Shigeki Higashiyama,[6] Masayuki Endoh,[4] Yasufumi Kaneda,[4] Satoshi Takagi,[5] Satoshi Itami,[5] Naoki Takeda,[7] Gen Yamada,[7] and Eisuke Mekada[1]

[1]Research Institute for Microbial Diseases, Osaka University, Osaka 565-0871, Japan
[2]Medical Institute of Bioregulation, Kyushu University, Fukuoka 812-8582, Japan
[3]Department of Internal Medicine and Therapeutics, [4]Division of Gene Therapy Science, and [5]Department of Dermatology, Graduate School of Medicine, Osaka University, Osaka 565-0871, Japan
[6]Department of Medical Biochemistry, Ehime University School of Medicine, Ehime 791-0295, Japan
[7]Center for Animal Resource and Development and Graduate School of Molecular and Genomic Pharmacy, Kumamoto University, Kumamoto 860-0811, Japan

Heparin-binding EGF-like growth factor (HB-EGF) is first synthesized as a membrane-anchored form (proHB-EGF), and its soluble form (sHB-EGF) is released by ectodomain shedding from proHB-EGF. To examine the significance of proHB-EGF processing in vivo, we generated mutant mice by targeted gene replacement, expressing either an uncleavable form (HB^{uc}) or a transmembrane domain–truncated form ($HB^{\Delta tm}$) of the molecule. $HB^{uc/uc}$ mice developed severe heart failure and enlarged heart valves, phenotypes similar to those in proHB-EGF null mice. On the other hand, mice carrying $HB^{\Delta tm}$ exhibited severe hyperplasia in both skin and heart. These results indicate that ectodomain shedding of proHB-EGF is essential for HB-EGF function in vivo, and that this process requires strict control.

Introduction

Heparin-binding EGF-like growth factor (HB-EGF), a member of the EGF family, binds the EGF receptor (EGFR) and ErbB4 to initiate signaling (Higashiyama et al., 1991; Elenius et al., 1997). Like other EGF family members (for review see Massague and Pandiella, 1993), HB-EGF is first synthesized as a membrane-anchored form (proHB-EGF), and then the soluble form (sHB-EGF) is released from the cell surface by ectodomain shedding (Goishi et al., 1995). sHB-EGF is a diffusible factor with potent mitogenic and chemoattractant activities for a number of cell types. ProHB-EGF forms a complex with other membrane proteins at the cell–cell contact site and transduces biological signals to neighboring cells in a nondiffusible manner (for review see Iwamoto and Mekada, 2000). Thus, in addition to being a precursor of sHB-EGF, proHB-EGF is thought to be a biologically active molecule itself. Several studies in vitro have revealed that a number of signaling molecules control the ectodomain shedding of proHB-EGF (Izumi et al., 1998; Umata et al., 2001; Takenobu et al., 2003), implying that strict control of ectodomain shedding is critical for HB-EGF function.

Recently, we demonstrated that HB-EGF is critical for proper heart development and function by the analyses of HB-EGF null mice (Iwamoto et al., 2003). However, it remains unclear which forms of HB-EGF are necessary for these process. The relative roles of either proHB-EGF or sHB-EGF and the significance of the control of ectodomain shedding in vivo have yet to be determined. To address these issues, we generated two kinds of mutant mice, by targeted gene replacement, that express either an uncleavable (HB^{uc}) or a transmembrane domain–truncated form ($HB^{\Delta tm}$) of proHB-EGF. Analysis of these mutant lines indicates that

S. Yamazaki and R. Iwamoto contributed equally to this work.

The online version of this article includes supplemental material.

Address correspondence to Eisuke Mekada, Department of Cell Biology, Research Institute for Microbial Diseases, Osaka University, Osaka 565-0871, Japan. Tel.: 81-6-6879-8286. Fax: 81-6-6879-8289. email: emekada@biken.osaka-u.ac.jp

Key words: ectodomain shedding; ErbB; cardiomyopathy; valvulogenesis; epidermal hyperplasia

Abbreviations used in this paper: EGFR, EGF receptor; HB-EGF, heparin-binding EGF-like growth factor; proHB-EGF, membrane-anchored form of HB-EGF; sHB-EGF, soluble form of HB-EGF; TPA, *O*-tetradecanoylphorbol-13-acetate; tRA, all-trans retinoic acid.

The Journal of Cell Biology, Volume 163, Number 3, November 10, 2003 469–475
http://www.jcb.org/cgi/doi/10.1083/jcb.200307035

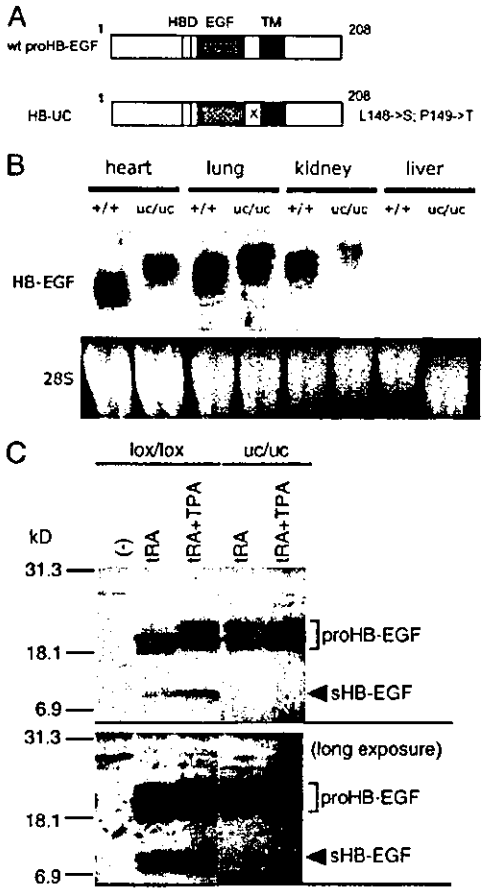

Figure 1. **Expression and uncleavability of HB-UC in HB^{uc} knock-in mice.** (A) Schematic structures of the HB-UC constructs. HBD, heparin-binding domain; EGF, EGF-like domain; TM, transmembrane domain. (B) Northern blot analysis of HB-EGF mRNA from adult WT (+/+) and HB$^{uc/uc}$ (uc/uc) mice. The size of the transcript from HB^{uc} is 100 bp larger than that from the WT gene due to neo cassette integration. (C) Uncleavable HB-UC in tRA- and TPA-treated skin. HB-EGF immunoblots of protein extracted and concentrated by heparin-Sepharose from 11-wk-old control (lox/lox) or HB$^{uc/uc}$ (uc/uc) mouse skin, treated with tRA (tRA), TPA after tRA treatment (tRA + TPA), or no treatment (−).

proHB-EGF shedding is essential in vivo and that this process must be controlled.

Results and discussion

Generation of mice expressing uncleavable proHB-EGF mutant

An uncleavable form of proHB-EGF was generated by creating double point mutations, L148S/P149T, in the juxtamembrane domain (designated HB^{uc}) (Fig. 1 A). As shown previously in cases of each single point mutation (Hirata et al., 2001), HB-UC (a product of HB^{uc}) was also resistant to ectodomain shedding in response to various shedding-inducing stimuli, while the other biological properties of HB-UC were similar to those of WT proHB-EGF (Fig. S1, A–C, and supplemental Results, available at http://www.jcb.org/cgi/content/full/jcb.200307035/DC1). To assess the biological significance of proHB-EGF ectodomain shedding, we created mutant mice expressing HB-UC instead of WT proHB-EGF by targeted replacement of the proHB-EGF gene with HB^{uc} cDNA (Fig. S2, supplemental Results, and supplemental Materials and methods, available at http://www.jcb.org/cgi/content/full/jcb.200307035/DC1). Homozygous mice (HB$^{uc/uc}$) were born at the predicted Mendelian frequency. Northern blotting of the transcripts obtained from adult mice indicated that the WT and HB^{uc} alleles were expressed equally in heart, lung, and kidney (Fig. 1 B).

We examined whether HB-UC was resistant to ectodomain shedding in mice (Fig. 1 C). We used adult mouse skin samples obtained from HB$^{uc/uc}$ mice and HB$^{lox/lox}$ mice as a control. In HB$^{lox/lox}$ mice, the proHB-EGF locus was replaced with WT proHB-EGF cDNA (Iwamoto et al., 2003), making HB$^{lox/lox}$ mice more suitable controls than WT mice. In adult mouse skin, HB-EGF protein bands were hardly detected in samples obtained from adult HB$^{uc/uc}$ and HB$^{lox/lox}$ mice. All-trans retinoic acid (tRA) is known to induce HB-EGF expression, followed by epidermal hyperplasia (Xiao et al., 1999). When tRA was applied to skin on the backs of mice, proHB-EGF protein was induced and clearly detected in samples from HB$^{lox/lox}$ and HB$^{uc/uc}$ mice by using an antibody against the proHB-EGF ectodomain. Under these conditions, the band corresponding to sHB-EGF was also detected in HB$^{lox/lox}$ mice, but not in HB$^{uc/uc}$ mice. An antibody recognizing the cytoplasmic domain of proHB-EGF did not detect this sHB-EGF band (unpublished data), confirming that this band corresponds to secreted HB-EGF. When tRA-induced skin was further treated with *O*-tetradecanoylphorbol-13-acetate (TPA), the sHB-EGF band appeared more intensely in HB$^{lox/lox}$ mice. However, the sHB-EGF band was not detected in samples from tRA + TPA–treated HB$^{uc/uc}$ mice. These results indicate that ectodomain shedding of proHB-EGF is severely impaired in HB$^{uc/uc}$ mice.

Uncleavable proHB-EGF mutation causes cardiac dysfunction and heart valve malformation

Recently, we showed that HB-EGF null mice (HB$^{del/del}$) have defects in cardiac chamber dilation and cardiac valve malformation (Iwamoto et al., 2003). Therefore, we analyzed the heart phenotype in HB$^{uc/uc}$ mice. Autopsies of HB$^{uc/uc}$ mice revealed massive enlargement of the heart. Histological analysis showed that wall thickness was reduced, accompanied by sporadic fibrosis in 12-wk-old HB$^{uc/uc}$ mice (Fig. 2, A–D). These phenotypes are highly similar to those observed in HB-EGF null mice (Iwamoto et al., 2003) and ErbB2 conditional knockout mice (Crone et al., 2002; Ozcelik et al., 2002).

Transthoracic echocardiography indicated marked dilation and poor left ventricular contraction in HB$^{uc/uc}$ mice (Fig. 2, E and F). Dilation could be detected in 4-wk-old mice, though the physical activity level and appearance was indistinguishable between WT and HB$^{uc/uc}$ mice. Mutant mice also had reduced cardiac wall movement, and ventricular fractional shortening (FS), a representative measure of systolic function, was greatly reduced.

In addition to the ventricular chamber abnormality, heart valve malformation was also observed in HB$^{uc/uc}$ mice as in HB-EGF null mice (Iwamoto et al., 2003; Jackson et al.,

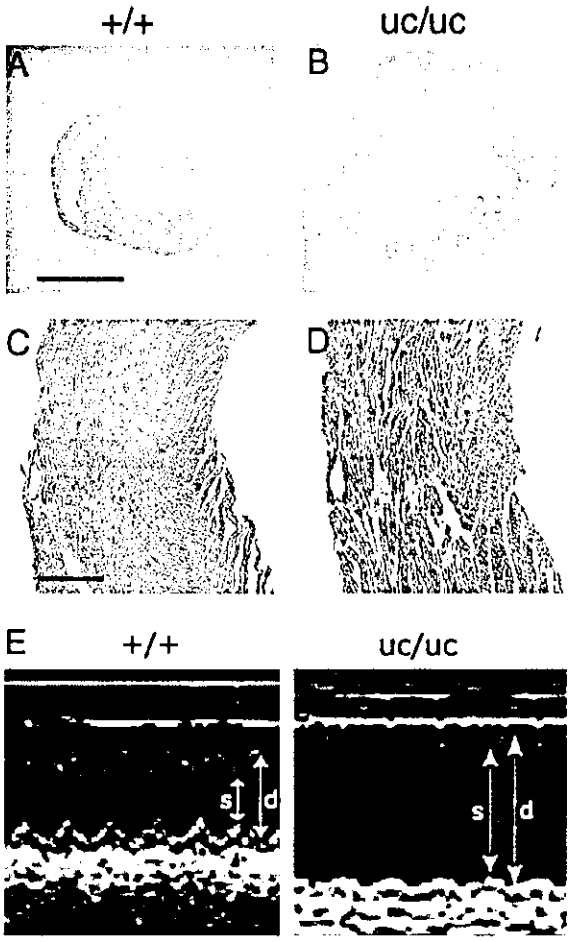

F

	+/+ (n=10)	uc/uc (n=13)	p-value
HR (/min)	630.9±79.3	644.0±60.1	n.s
sBP (mmHg)	102.3±6.4	93.3±8.1	p<0.05
dBP (mmHg)	64.4±7.8	55.4±6.4	p<0.05
LVDd (mm)	3.17±0.24	4.86±0.73	p<0.001
LVDs (mm)	2.04±0.29	3.80±0.84	p<0.001
FS (%)	35.7±4.8	22.5±7.3	p<0.001

Figure 2. **Histological and echocardiographic analysis of hearts from adult HB$^{uc/uc}$ mice.** (A and B) Hematoxylin-eosin staining of transverse sections through hearts of 12-wk-old mice at the papillary muscle level. Bar, 3 mm. (C and D) High magnification pictures. Sections were stained with Azan-Mallory. Massive fibrosis (blue stain) is present in 12-wk-old HB$^{uc/uc}$ heart throughout the vessel wall. Bar, 250 μm. (E and F) Echocardiographic analyses of hearts from WT (+/+) and HB$^{uc/uc}$ (uc/uc) mice. (E) Representative images of M-mode analyses are shown. Arrows indicate end-diastolic (d) and end-systolic (s) dimensions, respectively. (F) Physiological parameters of WT versus HB$^{uc/uc}$ hearts in 12-wk-old mice. HR, heart rate; sBP and dBP, systolic and diastolic blood pressure; LVDd and LVDs, left ventricular end diastolic and end systolic internal dimensions; FS, percent fractional shortening calculated as [(LVDd − LVDs)/LVDd] × 100. All values ± SEM.

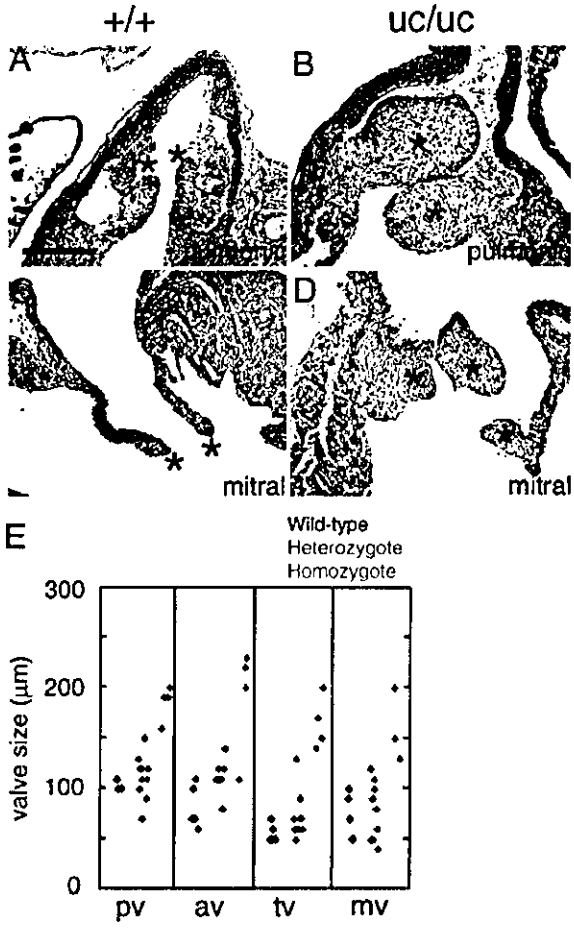

Figure 3. **Cardiac valve defects in HB$^{uc/uc}$ mice.** (A–D) Histological analysis of cardiac valves. Shown are hematoxylin-eosin–stained longitudinal sections of hearts of E17.5 embryos. Mice are WT (A and C) and HB$^{uc/uc}$ (B and D). Pulmonic (A and B) and mitral valves (C and D) are indicated by asterisks. Aortic and tricuspid valves were also enlarged (not depicted). Bar, 150 μm. (E) Measurement of cardiac valve size. The largest diameters of each valve in serial sections of E17.5 embryos of WT (black dots, $n = 5$), HB$^{uc/+}$ (blue dots, $n = 9$), and HB$^{uc/uc}$ (red dots, $n = 4$) hearts were measured. pv, pulmonic valve; av, aortic valve; tv, tricuspid valve; mv, mitral valve.

2003) and EGFR knockout mice (Chen et al., 2000). Histological analysis of E17.5 embryonic HB$^{uc/uc}$ hearts showed enlarged semilunar (aortic and pulmonic) and atrioventricular (mitral and tricuspid) valves (Fig. 3, A–D). Scoring of cardiac valve size in E17.5 hearts revealed enlarged semilunar and atrioventricular valves in HB$^{uc/uc}$ mice (Fig. 3 E). No overt abnormality was observed in HB$^{lox/lox}$ heart chambers or valves (Iwamoto et al., 2003), indicating that heart abnormalities in HB$^{uc/uc}$ mice were not due to a nonspecific effect of cDNA knock-in.

The similar heart defects displayed in HB$^{del/del}$ and HB$^{uc/uc}$ mice indicate that the process of ectodomain shedding is essential for HB-EGF function in normal cardiac valve development and cardiomyocyte function, and that soluble HB-EGF is required for these processes. We also examined whether proHB-EGF has any in vivo physiological role aside from acting as the sHB-EGF precursor. Interestingly, HB$^{del/del}$ mice

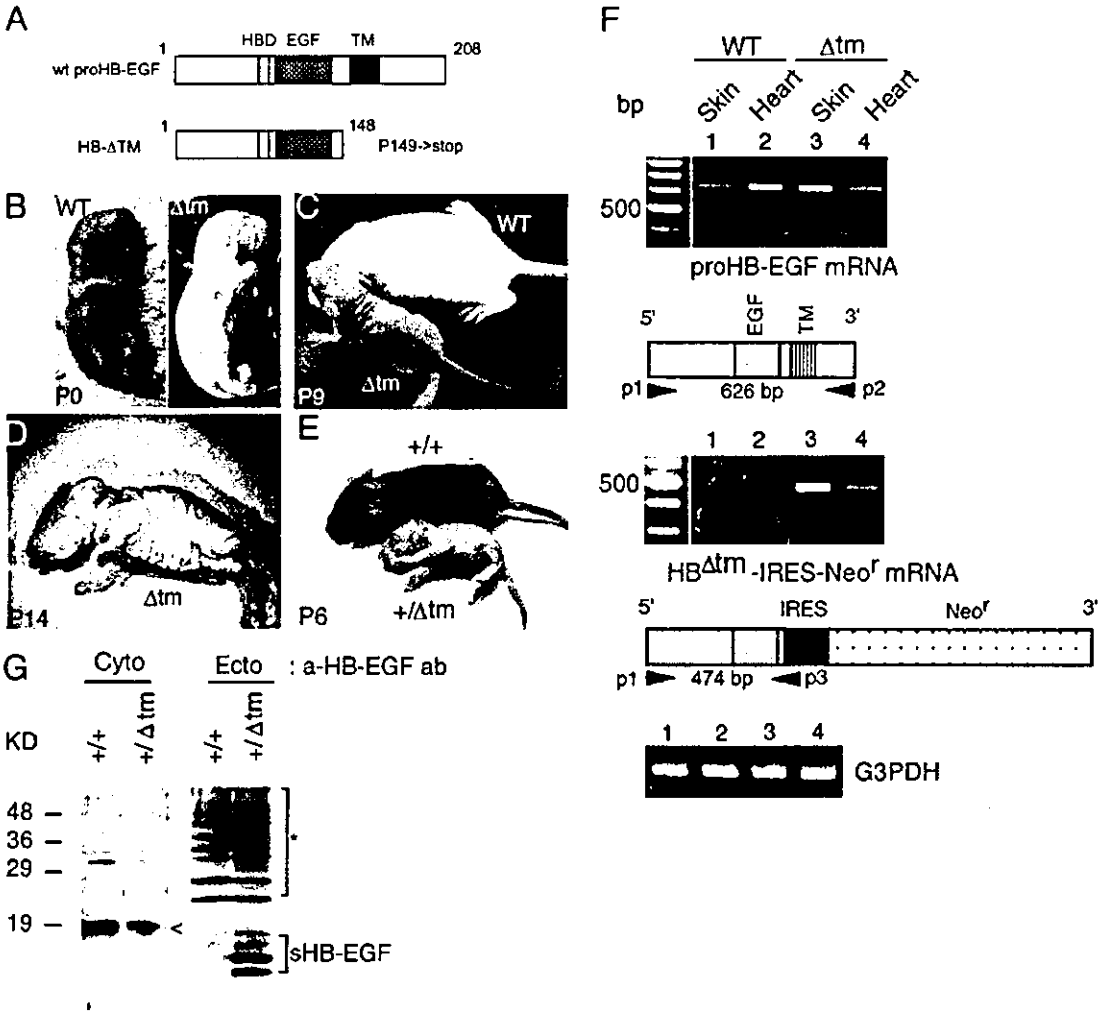

Figure 4. **$HB^{\Delta tm}$ knock-in mice.** (A) Schematic structures of the HB-ΔTM construct. (B–D) Phenotype of $HB^{\Delta tm}$ chimeric mice. P0 (B) and P9 (C) wild-type (WT) and $HB^{\Delta tm}$ chimeric (Δtm) mice and P14 $HB^{\Delta tm}$ chimeric mice (D) are shown. (E) Phenotype of P6 $HB^{\Delta tm}$ heterozygous mice (+/Δtm) and wild-type littermates (+/+). (F and G) Expression of $HB^{\Delta tm}$ in the targeted mice. (F) Transcription of the $HB^{\Delta tm}$ allele was assessed by RT-PCR analysis of tissues (skin and heart) from P14 wild-type (WT) and chimeric (Δtm) mice. Primer sets detecting the wild-type (p1 and p2) or $HB^{\Delta tm}$ allele (p1 and p3) transcripts are indicated below each gel. EGF, EGF-like domain; TM, transmembrane domain. RT-PCR with primer sets for the detection of GAPDH transcripts is shown in the lower panel as a loading control. (G) Detection of sHB-EGF in the skin. Immunoblots of proteins (150 μg/lane) extracted from P1 WT (+/+) or heterozygous (+/Δtm) mouse skin were performed using anti–proHB-EGF antibodies that recognize either intracellular (Cyto) or extracellular regions (Ecto) of HB-EGF. The extracellular-specific antibody detects sHB-EGF more efficiently than proHB-EGF. Four major bands corresponding to sHB-EGF, resulting from multiple processing and glycosylation sites in the HB-EGF NH_2-terminal region, were detected in $HB^{\Delta tm}$ heterozygous mice. Arrowheads indicate the bands corresponding to proHB-EGF. The asterisk indicates nonspecific bands.

displayed a shorter life span than $HB^{uc/uc}$ mice. Half of $HB^{uc/uc}$ mice survive over 18 wk, while >60% of $HB^{del/del}$ mice died in the first postnatal week. These differences between $HB^{del/del}$ and $HB^{uc/uc}$ mice suggest that proHB-EGF may function in unidentified developmental processes. Further comparison of the phenotypes between $HB^{del/del}$ and $HB^{uc/uc}$ mice may help us answer this question.

Generation of mice expressing soluble proHB-EGF mutant

Although studies of $HB^{uc/uc}$ mice indicated that ectodomain shedding of proHB-EGF and release of sHB-EGF is necessary for proper HB-EGF function in vivo, the physiological importance of the control of proHB-EGF ectodomain shedding remained unclear. To address this issue, we prepared another mouse mutant that only expresses sHB-EGF. The transmembrane domain–truncated mutant ($HB^{\Delta tm}$) was generated by insertion of a stop codon between Leu^{148} and Pro^{149} (Fig. 4 A), the major site for proHB-EGF processing (Higashiyama et al., 1992). Mitogenic activity was similar between HB-ΔTM (product of $HB^{\Delta tm}$) and WT sHB-EGF derived from proHB-EGF shedding, but HB-ΔTM is secreted at much higher levels than WT sHB-EGF (Fig. S1, D–G, and supplemental Results). The targeting construct

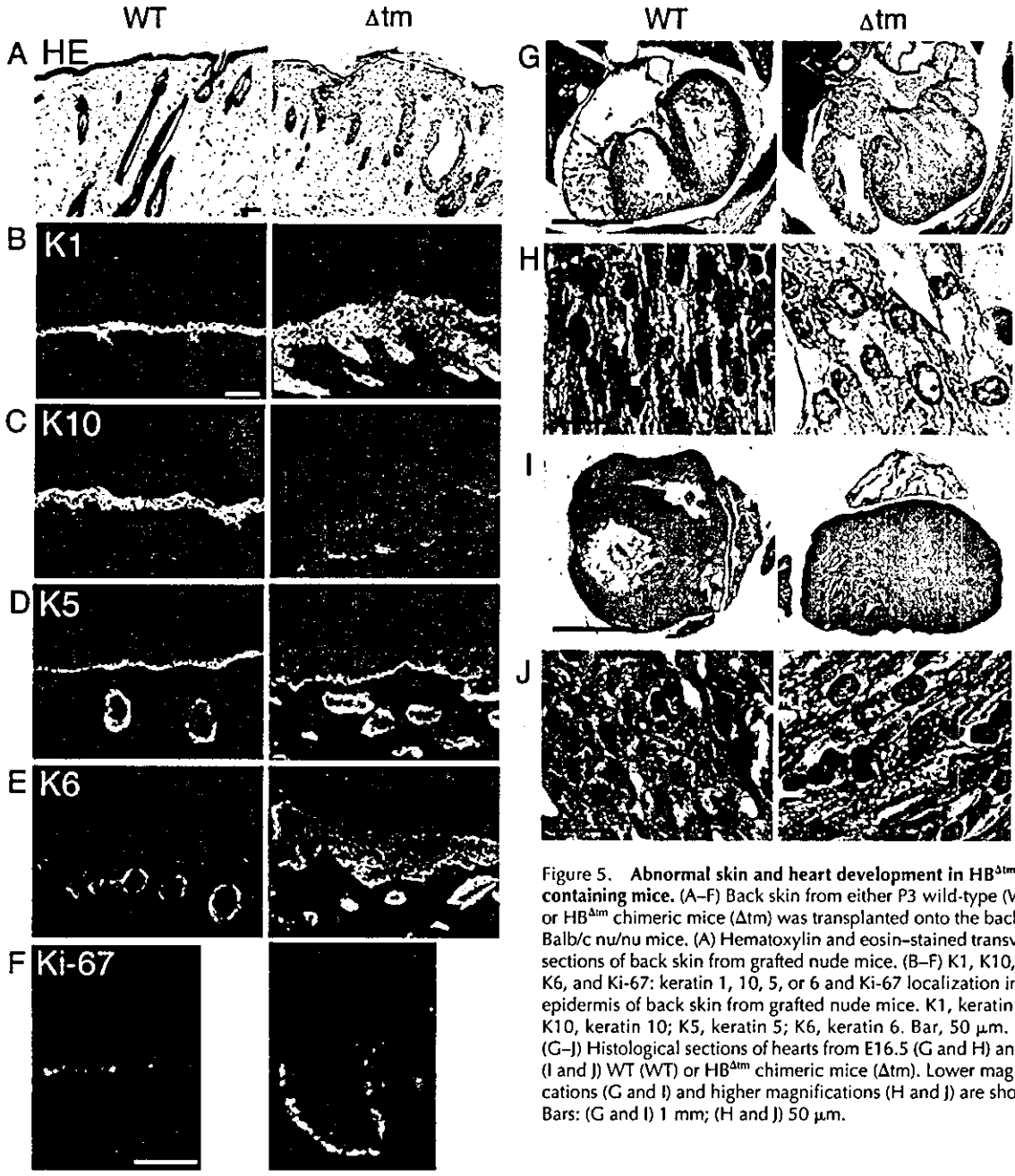

Figure 5. **Abnormal skin and heart development in HB$^{\Delta tm}$-containing mice.** (A–F) Back skin from either P3 wild-type (WT) or HB$^{\Delta tm}$ chimeric mice (Δtm) was transplanted onto the backs of Balb/c nu/nu mice. (A) Hematoxylin and eosin–stained transverse sections of back skin from grafted nude mice. (B–F) K1, K10, K5, K6, and Ki-67: keratin 1, 10, 5, or 6 and Ki-67 localization in the epidermis of back skin from grafted nude mice. K1, keratin 1; K10, keratin 10; K5, keratin 5; K6, keratin 6. Bar, 50 μm. (G–J) Histological sections of hearts from E16.5 (G and H) and P0 (I and J) WT (WT) or HB$^{\Delta tm}$ chimeric mice (Δtm). Lower magnifications (G and I) and higher magnifications (H and J) are shown. Bars: (G and I) 1 mm; (H and J) 50 μm.

for HB$^{\Delta tm}$ is similar to that for HB^{uc}. One allele of the proHB-EGF gene in ES cells was replaced with HB$^{\Delta tm}$ through homologous recombination (Fig. S2, supplemental Results, and supplemental Materials and methods). Chimeric mice carrying HB$^{\Delta tm}$ were generated from these ES clones. Most chimeric founders exhibited abnormally small bodies and thickened skin (Fig. 4, B–D). The majority of these mice died before or during the neonatal stage (unpublished data). A few mice, however, survived and were fertile. Most of the resulting F1 heterozygotes carrying the HB$^{\Delta tm}$ allele also died before or during the neonatal stage (unpublished data), displaying a more severe phenotype than that seen in chimeric mice (Fig. 4 E).

We confirmed the expression of the HB$^{\Delta tm}$ cDNA in chimeric mice by RT-PCR of skin and heart specimens (Fig. 4 F). Transcripts derived from the WT proHB-EGF allele were detected in both WT and chimeric tissues, while those derived from the HB$^{\Delta tm}$ allele were only identified in chimeric mice. Expression of HB$^{\Delta tm}$ was also confirmed at the protein level using anti–HB-EGF antibody, specific for the extracellular domain of proHB-EGF. In heterozygote skin, significant quantities of soluble HB-EGF were detected, whereas sHB-EGF protein was only barely detectable in WT skin (Fig. 4 G). The quantities of proHB-EGF with a molecular mass of ~19 kD, detected by an anti–HB-EGF antibody specific for the cytoplasmic domain, displayed a con-

comitant decrease in heterozygote skin relative to the levels seen in wild-type skin (Fig. 4 G).

Dysregulated release of HB-EGF induces developmental abnormalities with hyperplasia

The most obvious phenotype of $HB^{\Delta tm}$-carrying mice, distinguishing them from WT mice, was the presence of abnormal elephant-like skin (Figs. 4, B–E). $HB^{\Delta tm}$ mice have short lives; thus to further study the epidermal hyperplasia, back skin was transplanted from P3 WT or $HB^{\Delta tm}$ chimeric mice onto the backs of Balb/c nu/nu mice for 2 wk. This transplantation method also allowed for the specific examination of the effects of $HB^{\Delta tm}$ in the skin in an animal with otherwise normal expression and processing of HB-EGF. Histological examination revealed severe epidermal hyperplasia, accompanied by the presence of large, disorganized, hair follicle–like structures (Fig. 5 A). Immunohistochemistry of epidermal marker proteins revealed perturbed differentiation and proliferation of keratinocytes (Fig. 5, B–F). Keratin 5, normally expressed by both mitotically active, basal layer keratinocytes and hair follicles, was detected in the suprabasal epidermis of chimeric mice (Fig. 5 D). Keratin 1, normally expressed by differentiating keratinocytes in the suprabasal epidermis, but not by the cells of the hair follicle (Heid et al., 1988), was expressed in the hair follicle–like structures of chimeric mice (Fig. 5 B). Additionally, keratin 10, a differentiating keratinocyte marker, was down-regulated in chimeric mice (Fig. 5 C). Keratin 6, expressed predominantly in hair follicle cells, and at lower levels in the suprabasal epidermis, was detected throughout the epidermis of chimeric mice (Fig. 5 E), consistent with the induction of keratin 6 expression by epidermal hyperproliferation (Werner et al., 1993). The expression of Ki-67, a nuclear mitotic marker, was also increased in the basal layer of chimeric skin compared with levels seen in WT (Fig. 5 F), indicating that $HB^{\Delta tm}$ expression accelerates basal layer keratinocyte proliferation. No overt abnormality was observed in the skin area surrounding the transplanted skin, suggesting that the abnormality in the transplanted skin is due to the action of HB-ΔTM in a manner of autocrine or paracrine in limited distance, rather than paracrine in long distance.

Morphological abnormalities were also found in the heart of $HB^{\Delta tm}$ mice. Histological specimens showed ventricular hypertrophy in hearts from $HB^{\Delta tm}$ E16.5 embryos (Fig. 5 G) and P0 mice (Fig. 5 I). HB-EGF is expressed in cardiomyocytes (Iwamoto et al., 2003), consistent with the present results. The cardiac muscle fibers in chimeric mice were loose, with enlarged nuclei (Fig. 5, H and J). These results suggest that expression of $HB^{\Delta tm}$ reduces cardiomyocyte differentiation or terminates proliferation. These cardiac developmental abnormalities may be the primary cause of early death in $HB^{\Delta tm}$ mice.

The phenotype observed in $HB^{\Delta tm}$ mice is likely due to dysregulated secretion of sHB-EGF. In normal conditions, a portion of proHB-EGF molecules are converted to sHB-EGF, but the majority of proHB-EGF molecules on the cell surface seems to be internalized without shedding (Goishi et al., 1995). In the case of $HB^{\Delta tm}$, most synthesized molecules would be secreted without shedding, resulting in oversecretion of sHB-EGF even though the native HB-EGF promoter regulates gene expression. Therefore, dysregulated secretion of sHB-EGF would result in severe developmental abnormalities. The present study thus confirms the notion that ectodomain shedding of proHB-EGF must be strictly controlled in vivo.

One question regarding the truncated $HB^{\Delta tm}$ mutant concerns whether the observed hyperplasia might be due to an intracrine rather than a paracrine mechanism. A transmembrane domain–truncated EGF mutant was reported to activate EGFR in an intracrine manner, as a result of interaction with EGFR within cytoplasmic vesicles, before the molecules reached the cell surface (Wiley et al., 1998). However, this was not the case for HB-EGF. We have performed ex vivo transfection of $HB^{\Delta tm}$ cDNA into mouse embryonic skin (Fig. S3 and supplemental Results, available at http://www.jcb.org/cgi/content/full/jcb.200307035/DC1). Transfection of $HB^{\Delta tm}$, but not WT proHB-EGF, resulted in embryonic epidermal hyperplasia. CRM197, a protein that specifically inhibits the mitogenic activity of HB-EGF (Mitamura et al., 1995), inhibited HB-ΔTM–induced hyperplasia. As CRM197 is membrane impermeable, hyperplasia induced by transfection with $HB^{\Delta tm}$ must be mediated by secreted HB-ΔTM in a paracrine manner.

In conclusion, proHB-EGF shedding and the strict control of this process are essential for the function of this growth factor. Not only HB-EGF, but also other EGF family growth factors and cytokines are synthesized as membrane-anchored forms. The present study suggests that the strict control of ectodomain shedding is essential for the physiological function of these membrane-anchored ligands. This study also indicates that posttranslational regulation, in addition to transcriptional control, is crucial for the function of membrane-anchored growth factors.

Materials and methods

Northern blotting

Total RNA was isolated from tissues using ISOGEN (Nippon Gene), according to the manufacturer's instructions. Details of the hybridization procedure are shown in the supplemental Materials and methods (available at http://www.jcb.org/cgi/content/full/jcb.200307035/DC1).

Immunoblotting of tissues

For the detection of HB-EGF and HB-UC in adult skin, back skin from 11-wk-old $HB^{lox/lox}$ and $HB^{uc/uc}$ mice was treated with 800 nmol of tRA for 3 d. 2 h before specimen isolation, the back skin was additionally treated with 8 nmol of TPA. The isolated full back skin was homogenized in lysis buffer (Iwamoto et al., 2003). For detection of HB-ΔTM in neonatal skin, skin from P1 $HB^{\Delta tm}$ heterozygous mice or WT littermates was homogenized in lysis buffer. Details of the immunoblotting procedure using these lysate samples are shown in the supplemental Materials and methods (available at http://www.jcb.org/cgi/content/full/jcb.200307035/DC1).

Histological analysis

Mouse hearts were fixed by perfusion with 4% paraformaldehyde, dehydrated, and embedded in paraffin. 4-μm sections were stained with either hematoxylin-eosin or Azan-Mallory. For immunohistochemical analysis of transplanted skin, specimens of full-thickness skin (2–3 cm^2) were transplanted onto the backs of Balb/c nu/nu mice (8 wk old) and then fixed with adhesive bandages for 1 wk. 2 wk after transplantation, skin specimens were isolated from the grafted skin and subjected to immunohistochemical analysis. Information of the used antibodies for immunohistochemistry, microscopy, and image processing is shown in the supplemental Materials and methods (available at http://www.jcb.org/cgi/content/full/jcb.200307035/DC1).

Echocardiography

Transthoracic echocardiograph was performed with a cardiac ultrasound recorder (SONOS 5500; Hewlett-Packard) with a 15-MHz transducer, as described previously (Iwamoto et al., 2003).

RT-PCR

RNA was isolated from tissues of P14 mice using TRIzol reagent (Invitrogen). Reverse transcription was performed using a reverse transcriptase, ReverTra Dash (TOYOBO). Primer sets used in PCR analyses are shown in the supplemental Materials and methods (available at http://www.jcb.org/cgi/content/full/jcb.200307035/DC1).

Online supplemental material

The supplemental material is available at http://www.jcb.org/cgi/content/full/jcb.200307035/DC1. Fig. S1 shows the characterizations of HB-UC and HB-ΔTM. Fig. S2 shows the targeting construct of HB^{UC} and $HB^{\Delta tm}$ and genotypic analyses. Fig. S3 shows ex vivo transfection of $HB^{\Delta tm}$ cDNA into mouse embryonic skin. Supplemental Results, Materials and methods, and References are also presented.

We thank I. Ishimatsu, M. Hamaoka, and T. Yoneda for technical assistance.

This work was supported by the Research for the Future Program of the Japan Society for the Promotion of Science (97L00303 for E. Mekada) and by Grants-in-Aid from the Ministry of Education, Culture, Sports, Science, and Technology (12215152 and 14032202 for E. Mekada and 12680705 for R. Iwamoto).

Submitted: 7 July 2003
Accepted: 12 September 2003

References

Chen, B., R.T. Bronson, L.D. Klaman, T.G. Hampton, J.F. Wang, P.J. Green, T. Magnuson, P.S. Douglas, J.P. Morgan, and B.G. Neel. 2000. Mice mutant for Egfr and Shp2 have defective cardiac semilunar valvulogenesis. *Nat. Genet.* 24:296–299.

Crone, S.A., Y.Y. Zhao, L. Fan, Y. Gu, S. Minamisawa, Y. Liu, K.L. Peterson, J. Chen, R. Kahn, G. Condorelli, et al. 2002. ErbB2 is essential in the prevention of dilated cardiomyopathy. *Nat. Med.* 8:459–465.

Elenius, K., S. Paul, G. Allison, J. Sun, and M. Klagsbrun. 1997. Activation of HER4 by heparin-binding EGF-like growth factor stimulates chemotaxis but not proliferation. *EMBO J.* 16:1268–1278.

Goishi, K., S. Higashiyama, M. Klagsbrun, N. Nakano, T. Umata, M. Ishikawa, E. Mekada, and N. Taniguchi. 1995. Phorbol ester induces the rapid processing of cell surface heparin-binding EGF-like growth factor: conversion from juxtacrine to paracrine growth factor activity. *Mol. Biol. Cell.* 6:967–980.

Heid, H.W., I. Moll, and W.W. Franke. 1988. Patterns of expression of trichocytic and epithelial cytokeratins in mammalian tissues. II. Concomitant and mutually exclusive synthesis of trichocytic and epithelial cytokeratins in diverse human and bovine tissues (hair follicle, nail bed and matrix, lingual papilla, thymic reticulum). *Differentiation.* 37:215–230.

Higashiyama, S., J.A. Abraham, J. Miller, J.C. Fiddes, and M. Klagsbrun. 1991. A heparin-binding growth factor secreted by macrophage-like cells that is related to EGF. *Science.* 251:936–939.

Higashiyama, S., K. Lau, G.E. Besner, J.A. Abraham, and M. Klagsbrun. 1992. Structure of heparin-binding EGF-like growth factor. Multiple forms, primary structure, and glycosylation of the mature protein. *J. Biol. Chem.* 267: 6205–6212.

Hirata, M., T. Umata, T. Takahashi, M. Ohnuma, Y. Miura, R. Iwamoto, and E. Mekada. 2001. Identification of serum factor inducing ectodomain shedding of proHB-EGF and studies of noncleavable mutants of proHB-EGF. *Biochem. Biophys. Res. Commun.* 283:915–922.

Iwamoto, R., and E. Mekada. 2000. Heparin-binding EGF-like growth factor: a juxtacrine growth factor. *Cytokine Growth Factor Rev.* 11:335–344.

Iwamoto, R., S. Yamazaki, M. Asakura, S. Takashima, H. Hasuwa, K. Miyado, S. Adachi, M. Kitakaze, K. Hashimoto, G. Raab, et al. 2003. Heparin-binding EGF-like growth factor and ErbB signaling is essential for heart function. *Proc. Natl. Acad. Sci. USA.* 100:3221–3226.

Izumi, Y., M. Hirata, H. Hasuwa, R. Iwamoto, T. Umata, K. Miyado, Y. Tamai, T. Kurisaki, A. Sehara-Fujisawa, S. Ohno, and E. Mekada. 1998. A metalloprotease-disintegrin, MDC9/meltrin-γ/ADAM9 and PKCδ are involved in TPA-induced ectodomain shedding of membrane-anchored heparin-binding EGF-like growth factor. *EMBO J.* 17:7260–7272.

Jackson, L.F., T.H. Qiu, S.W. Sunnarborg, A. Chang, C. Zhang, C. Patterson, and D.C. Lee. 2003. Defective valvulogenesis in HB-EGF and TACE-null mice is associated with aberrant BMP signaling. *EMBO J.* 22:2704–2716.

Massague, J., and A. Pandiella. 1993. Membrane-anchored growth factors. *Annu. Rev. Biochem.* 62:515–541.

Mitamura, T., S. Higashiyama, N. Taniguchi, M. Klagsbrun, and E. Mekada. 1995. Diphtheria toxin binds to the epidermal growth factor (EGF)-like domain of human heparin-binding EGF-like growth factor/diphtheria toxin receptor and inhibits specifically its mitogenic activity. *J. Biol. Chem.* 270: 1015–1019.

Ozcelik, C., B. Erdmann, B. Pilz, N. Wettschureck, S. Britsch, N. Hubner, K.R. Chien, C. Birchmeier, and A.N. Garratt. 2002. Conditional mutation of the ErbB2 (HER2) receptor in cardiomyocytes leads to dilated cardiomyopathy. *Proc. Natl. Acad. Sci. USA.* 99:8880–8885.

Takenobu, H., A. Yamazaki, M. Hirata, T. Umata, and E. Mekada. 2003. The stress- and inflammatory cytokine-induced ectodomain shedding of heparin-binding epidermal growth factor-like growth factor is mediated by p38 MAPK, distinct from the 12-O-tetradecanoylphorbol-13-acetate- and lysophosphatidic acid-induced signaling cascades. *J. Biol. Chem.* 278:17255–17262.

Umata, T., M. Hirata, T. Takahashi, F. Ryu, S. Shida, Y. Takahashi, M. Tsuneoka, Y. Miura, M. Masuda, Y. Horiguchi, and E. Mekada. 2001. A dual signaling cascade that regulates the ectodomain shedding of heparin-binding epidermal growth factor-like growth factor. *J. Biol. Chem.* 276:30475–30482.

Werner, S., W. Weinberg, X. Liao, K.G. Peters, M. Blessing, S.H. Yuspa, R.L. Weiner, and L.T. Williams. 1993. Targeted expression of a dominant-negative FGF receptor mutant in the epidermis of transgenic mice reveals a role of FGF in keratinocyte organization and differentiation. *EMBO J.* 12: 2635–2643.

Wiley, H.S., M.F. Woolf, L.K. Opresko, P.M. Burke, B. Will, J.R. Morgan, and D.A. Lauffenburger. 1998. Removal of the membrane-anchoring domain of epidermal growth factor leads to intracrine signaling and disruption of mammary epithelial cell organization. *J. Cell Biol.* 143:1317–1328.

Xiao, J.H., X. Feng, W. Di, Z.H. Peng, L.A. Li, P. Chambon, and J.J. Voorhees. 1999. Identification of heparin-binding EGF-like growth factor as a target in intercellular regulation of epidermal basal cell growth by suprabasal retinoic acid receptors. *EMBO J.* 18:1539–1548.

nature
genetics

Lamr1 functional retroposon causes right ventricular dysplasia in mice

Yoshihiro Asano[1], Seiji Takashima[1], Masanori Asakura[1], Yasunori Shintani[1], Yulin Liao[1], Tetsuo Minamino[1], Hiroshi Asanuma[1], Shoji Sanada[1], Jiyoong Kim[2], Akiko Ogai[2], Tomi Fukushima[1], Yumiko Oikawa[1], Yasushi Okazaki[3], Yasufumi Kaneda[4], Manabu Sato[4], Jun-ichi Miyazaki[5], Soichiro Kitamura[2], Hitonobu Tomoike[2], Masafumi Kitakaze[2] & Masatsugu Hori[1]

Arrhythmogenic right ventricular dysplasia (ARVD) is a hereditary cardiomyopathy that causes sudden death in the young. We found a line of mice with inherited right ventricular dysplasia (RVD) caused by a mutation of the gene laminin receptor 1 (*Lamr1*). This locus contained an intron-processed retroposon that was transcribed in the mice with RVD. Introduction of a mutated *Lamr1* gene into normal mice by breeding or by direct injection caused susceptibility to RVD, which was similar to that seen in the RVD mice. An *in vitro* study of cardiomyocytes expressing the product of mutated *Lamr1* showed early cell death accompanied by alteration of the chromatin architecture. We found that heterochromatin protein 1 (HP1) bound specifically to mutant LAMR1. HP1 is a dynamic regulator of heterochromatin sites, suggesting that mutant LAMR1 impairs a crucial process of transcriptional regulation. Indeed, mutant LAMR1 caused specific changes to gene expression in cardiomyocytes, as detected by gene chip analysis. Thus, we concluded that products of the *Lamr1* retroposon interact with HP1 to cause degeneration of cardiomyocytes. This mechanism may also contribute to the etiology of human ARVD.

ARVD is a type of right ventricular cardiomyopathy characterized by the gradual loss of cardiomyocytes and compensatory replacement with either adipose or fibrous tissue. ARVD is a primary cause of sudden cardiac death in juveniles and athletes, but is difficult to diagnose before the onset of cardiac events. In Italy, ARVD accounts for 20% of all sudden deaths in individuals under 35 years old and 22% of sudden deaths in athletes[1]. The etiology of this disease is still unknown. Familial occurrence is reported in about 30% of individuals with ARVD. Six associated loci have been mapped: ARVD1, 14q23 (ref. 1); ARVD2, 1q42 (ref. 1); ARVD3, 14q12 (ref. 2); ARVD4, 2q32 (ref. 3); ARVD5, 3p23 (ref. 4); and ARVD6, 10p12 (ref. 5). The only gene identified so far is that underlying ARVD2, which corresponds to the cardiac ryanodine receptor gene and causes a condition with different features from those of the other forms of ARVD[6]. As in humans, a naturally occurring phenotype of RVD has been reported in dogs, cats and minks[7–10], but the genes responsible have not been identified.

We report here a new mouse model of ARVD: we identified a retroposon insertion encoding a mutant form of the nuclear protein laminin receptor 1 (LAMR1) by positional cloning. LAMR1 is one of the ribosomal proteins localized in the nucleus and involved in apoptosis[11,12]. We also report possible molecular mechanisms leading to ARVD.

RESULTS

Mouse model of ARVD

We found a mouse model of ARVD by chance during the screening of antidiabetic compounds with KK obese mice that were originally isolated on the basis of hyperglycemia[13,14]. The mouse strain, named KK/Rvd, developed severe RVD. Macroscopic examination of the heart of these mice at 8 weeks of age showed massive fibrosis of the entire right ventricular wall that never extended to the left ventricle (**Fig. 1a,b**). This resembles the histopathology of human ARVD. We found that the outer third of the right ventricular wall was replaced by fibrous tissue and that calcification also occurred (**Fig. 1c,d**). This degenerative process commenced at 6 weeks of age and was completed by 10 weeks of age. There was some variation in the distribution of affected cardiomyocytes, but penetrance of the phenotype was almost 100%. Histologically, degradation of cardiomyocytes and macrophage infiltration were observed at the border between the fibrosis and the viable myocardial tissue (**Fig. 1e,g**), indicating that cardiomyocyte degeneration proceeded from the outer part of the right ventricular wall to the inner part. This outer-inner progression of RVD is also characteristic of human ARVD. Thin fibrous tissue surrounded the degraded cardiomyocytes at the

[1]Department of Internal Medicine and Therapeutics, Osaka University Graduate School of Medicine, 2-2 A8 Yamadaoka, Suita, Osaka 565-0871, Japan. [2]Cardiovascular Division of Internal Medicine, National Cardiovascular Center, 5-7-1 Fujishirodai, Suita, Osaka 565-8565, Japan. [3]Laboratory for Genome Exploration Research Group, RIKEN Genomic Sciences Center (GSC), RIKEN Yokohama Institute, Yokohama, Kanagawa 230-0045, Japan. [4]Department of Gene Therapy Science, Osaka University Graduate School of Medicine, 2-2 Yamadaoka, Suita, Osaka 565-0871, Japan. [5]Department of Nutrition and Physiological Chemistry, Osaka University Graduate School of Medicine, 2-2 Yamadaoka, Suita, Osaka 565-0871, Japan. Correspondence should be addressed to M.K. (kitakaze@zf6.so-net.ne.jp) or S.T. (takasima@medone.med.osaka-u.ac.jp).

Published online 18 January 2004; doi:10.1038/ng1294

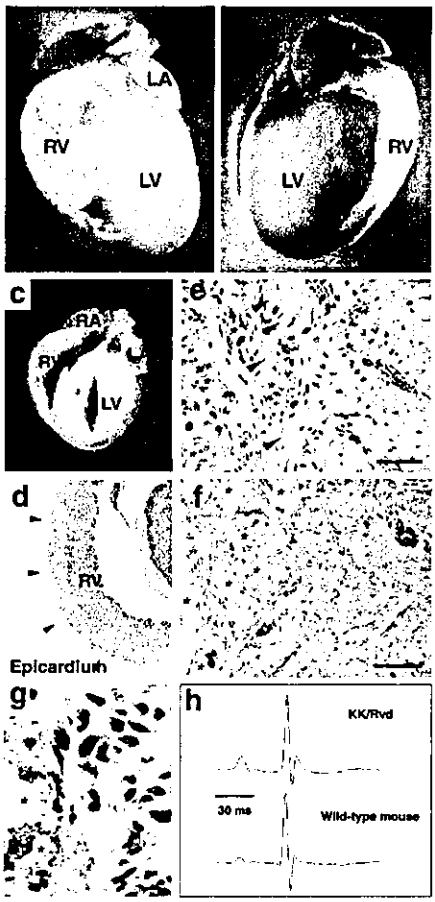

Figure 1 Massive fibrosis covers the outer side of the right ventricular wall, as with human ARVD, and never extends to the left ventricle. Macroscopic view of KK/Rvd mouse heart at 8 weeks old: (**a**) front view, (**b**) back view. (**c**,**d**) In the sagittal section, arrowheads indicate the degenerated area of the right ventricle. (**e**,**f**) At the borderline of the degenerated area (high magnification of yellow square in **d**), green arrows indicate the cardiomyocytes densely stained by eosin; yellow arrows indicate the degraded cardiomyocytes surrounded by fibrous tissue; asterisks indicate calcification. (**e**) Hematoxylin and eosin staining. (**f**) Masson-trichrome staining. (**g**) Infiltrating macrophages into a degraded area are stained by MCP-1 antibody. (**h**) Electrocardiography showed a prolonged QRS duration in KK/Rvd mice. LA, left atrium; LV, left ventricle; RA, right atrium; RV, right ventricle. Scale bars: **a**–**c**, 3 mm; **e**,**f**, 50 μm; **g**, 10 μm.

edge of the myocardial degeneration (**Fig. 1f**), indicating progressive replacement by fibrous tissue.

As lymphocyte infiltration was rarely observed, even when immunohistochemical staining was used (data not shown), autoimmune and infectious mechanisms were probably not involved. Detailed microscopic examination showed that the left ventricular myocardium was intact without any of the changes seen in the right ventricular myocardium. Electrocardiography showed a prolonged QRS duration (duration of ventricular muscle depolarization) in KK/Rvd mice compared with wild-type mice (**Fig. 1h**); this indicated a greater susceptibility to arrhythmia caused by intraventricular conduction disturbance. But electrocardiographic monitoring did not detect tachyarrhythmia, which is often seen in human ARVD. The other organs of these mice showed no histological abnormalities. Thus, KK/Rvd mice matched three of the primary clinical criteria for ARVD[15]: regional right ventricular dysplasia, inheritability and fibro-fatty replacement. Thus we concluded that this was an appropriate mouse model of human ARVD.

Identification of the locus underlying RVD

To investigate the mode of inheritance of RVD, we carried out a cross test between the wild-type PWK mouse strain and the KK/Rvd strain. F_1 mice showed no RVD, whereas the segregation ratio of normal to RVD mice among the F_2 and backcross progeny indicated that RVD was inherited as an autosomal recessive trait. We named the associated locus 'right ventricular dysplasia' (*rvd*). Linkage analysis of these backcross mice (n = 480) with the use of 165 microsatellite markers showed that the *rvd* locus was closely linked to *D7Mit270* near the middle of chromosome 7, with a maximum multipoint odds score of 4.67 (**Fig. 2a**). Using other markers deduced from the gene databases flanked with *D7Mit270*, we further genotyped these mice and localized the recombinants to a region of ~3.0 cM.

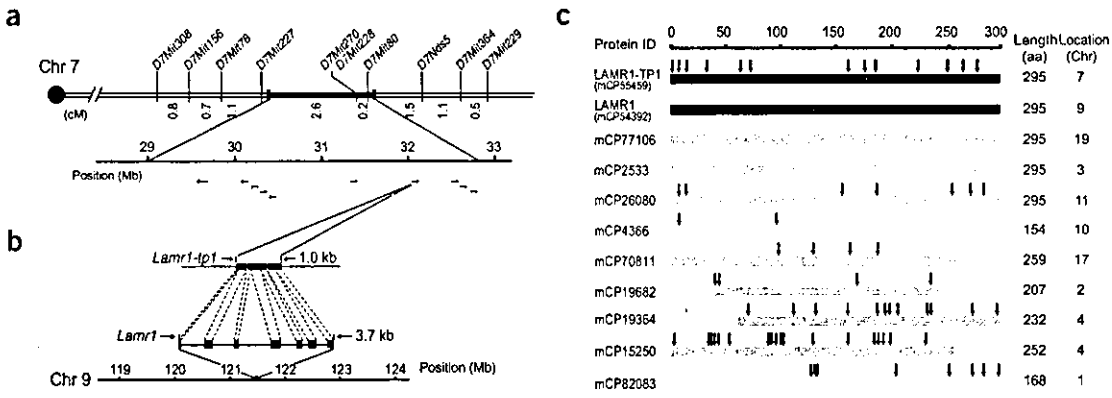

Figure 2 Location, alignment and expression of *Lamr1-tp1*. (**a**) The *rvd* locus was mapped to mouse chromosome 7, linking to *D7Mit270*. (**b**) Sequence of 1,031 bp was inserted in the KK/Rvd mouse genome but not in the PWK mouse genome. (**c**) Alignments of *Lamr1* retroposons in the mouse genome database and the comparison of translated amino acid (aa) sequences to the LAMR1 sequence (from the original *Lamr1* gene located in chromosome 9). Arrows indicate the amino acid transitions.

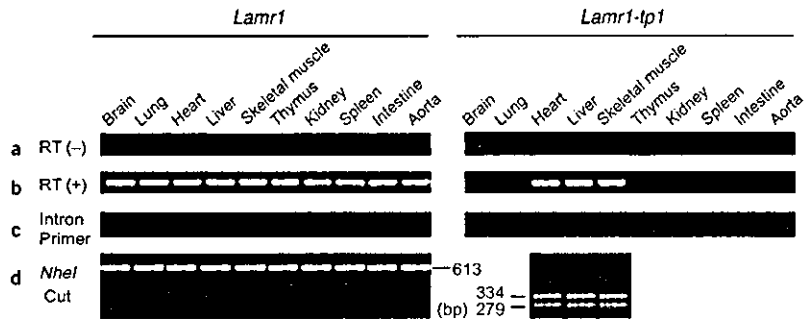

Figure 3 The expression of *Lamr1-tpl* was confirmed only in KK/Rvd heart, liver and skeletal muscle. (**a**) RT(–) indicates the use of RNA samples from KK/Rvd tissues as the PCR template before RT-PCR. PCR primers were designed to include either *Lamr1*- or *Lamr1-tpl*-specific mutated sequences. (**b**) RT(+) indicates the use of the cDNA samples after RT-PCR. The primers were the same as in **a**. (**c**) The same templates were used as in **b**, but reaction primers were designed in the intron lesion of *Lamr1* or up- or downstream of *Lamr1-tpl*. (**d**) PCR products of **b** were digested by the restriction enzyme *NheI*, whose recognition site exists only in *Lamr1-tpl*.

Then we sequenced the exons of the *rvd* locus in the gene database and compared the sequences between KK/Rvd and PWK mice. New differences between the two strains shown by this analysis were used as markers to narrow the candidate locus. Within the narrowed region (0.5 cM) we found a 1,031-bp insertion in the KK/Rvd genome that was not present in the PWK genome (**Fig. 2b**). This insert was a 1,031-bp retroposon that encoded mutated *Lamr1*, which we named *Lamr1-tpl* (laminin receptor 1, transposed paralog 1). There was neither an annotated area nor a dbEST matched area within ~1 Mb of this insertion, indicating that alteration of a nearby gene was probably not the cause of this phenotype and suggesting that *Lamr1-tpl* itself was responsible for RVD.

The original *Lamr1* gene consists of seven exons and six introns located on chromosome 9, and it comprises 32 variants of retroposons that are probably derived from a retrovirus. The alignments of these paralogs of *Lamr1* are shown (**Fig. 2c**). Almost all the retroposons have stop codons in the open reading frame and thus are probably not translated. But four *Lamr1* retroposons, including *Lamr1-tpl*, have the stop codon in the same position as the *Lamr1* cDNA. This suggests that these genes could be translated to produce proteins with various mutations. Among the four full-length retroposons, two genes have exactly the same sequence as *Lamr1* and two genes encode mutated *Lamr1* (one of these is *Lamr1-tpl* located on chromosome 7 in KK/Rvd mice and the other is located on chromosome 11). The protein encoded by *Lamr1-tpl* (LAMR1-TP1) shares 96% sequence identity with the protein encoded by *Lamr1* (LAMR1), resulting in the translation of a protein showing a 13–amino acid mutation.

Tissue expression of *Lamr1-tpl*

For *Lamr1-tpl* to cause ARVD, this retroposon would need to be transcribed in the hearts of KK/Rvd mice. We used specific RT-PCR to amplify *Lamr1-tpl* and *Lamr1* transcripts. We isolated RNA and treated it with DNase to eliminate contamination by genomic DNA before RT-PCR. We confirmed the absence of contamination using several PCR reactions with different pairs of intron primers. *Lamr1-tpl* mRNA could only be transcribed in the heart, liver and skeletal muscle of KK/Rvd mice, whereas *Lamr1* mRNA was expressed ubiquitously (**Fig. 3**). Also, *Lamr1-tpl* was not transcribed in any of the tissues of PWK mice or other wild-type (C57Bl/6) mice. There was no difference in the expression of *Lamr1-tpl* in the right ventricle and left ventricle, suggesting that an additional factor was necessary to cause the specific pathological changes associated with ARVD. Despite the high expression of *Lamr1-tpl* transcripts, no pathology was observed in the liver and skeletal muscle of KK/Rvd mice.

In vivo role of LAMR1-TP1

To confirm that the *Lamr1-tpl* transcripts were responsible for the ARVD phenotype, we carried out functional studies of LAMR1-TP1. We transfected a green fluorescent protein (GFP) coexpression plasmid (pIRES2EGFP-Lamr1-tp1 or pIRES2EGFP-Lamr1) into the hearts of C57Bl/6 mice by direct injection of DNA into the right ventricle as described[16]. Three weeks after transfection, we detected expression of LAMR1-TP1 along with massive right ventricular wall damage at the injected area. We observed GFP^+ cardiomyocytes transfected with pIRES2EGFP-Lamr1-tp1 in the zone of degeneration accompanied by fibrosis (**Fig. 4a–c**). The degeneration of transfected cardiomyocytes started 2 weeks after injection of the plasmid. Lymphocyte infiltration was rarely seen in the injected area, and the same changes were also observed in immunosuppressed severe-combined immunodeficient mice (data not shown), suggesting that autoimmunity was probably not involved in this tissue damage. On the other hand, the hearts injected with plasmid pIRES2EGFP-Lamr1

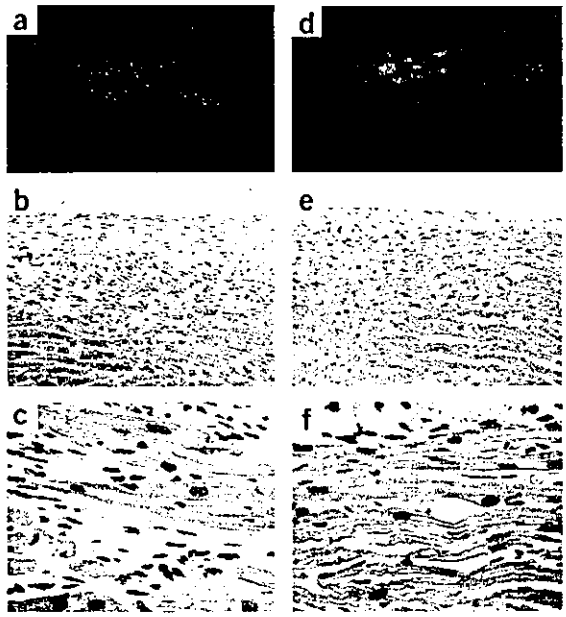

Figure 4 The direct gene injections showed the *Lamr1-tpl*-specific degradation of the myocardium. (**a,d**) GFP expression was detected in the gene-injected area. (**b,e**) Macroscopic view of transfected sites. (**c,f**) Magnified view of the transfected sites. (**a–c**) The vector pIRES2EGFP-Lamr1-tp1 was used. (**d–f**) The vector pIRES2EGFP-Lamr1 was used. Magnification: **a,d**, ×40; **b,e**, ×100; **c,f**, ×400.

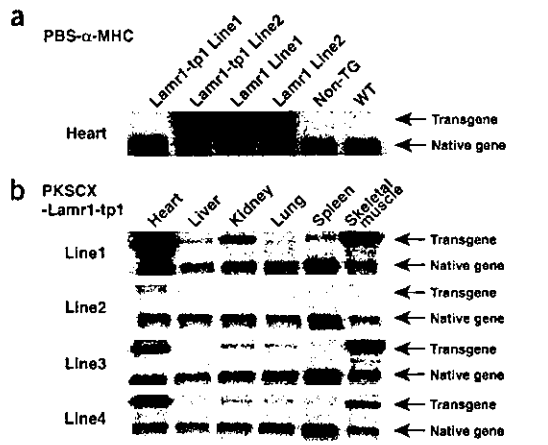

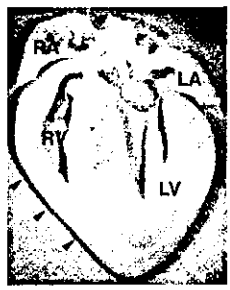

Figure 5 Expressional (northern blot) analysis both of the transgenes and native genes in each transgenic mouse model. *Lamr1-tp1* and *Lamr1* were detected in equal amounts in this analysis. (**a**) Transgene expression in heart samples from two strains of PBS-α-MHC-Lamr1-tp1 mice, two strains of PBS-α-MHC-Lamr1 mice and a control (WT) mouse strain. Non-TG, nontransgenic strain. (**b**) Comparison of gene expression by four lines of the transgenic mouse model PKSCX-Lamr1-tp1 in which transgenes were systemically expressed. (**c**) The complete change to the right ventricle is shown in a macroscopic view of a PBS-α-MHC-Lamr1-tp1 heart from a 10-week-old mouse. LA, left atrium; LV, left ventricle; RA, right atrium; RV, right ventricle.

showed only slight damage at the injection site and the GPF$^+$ cells were healthy, showing no degradation (**Fig. 4d–f**). Fibrous tissue was rarely seen in the hearts transfected with *Lamr1*.

We analyzed further the role of LAMR1-TP1 using transgenic mice. We generated two strains of transgenic mice that expressed *Lamr1* either systemically (with a KSCX promoter) or only in the heart (with an α-MHC promoter). We then established six substrains of *Lamr1-tp1* transgenic mice (four with KSCX promoters and two with α-MHC promoters) and four substrains of *Lamr1* transgenic mice (**Fig. 5a,b**). Among the six strains of *Lamr1-tp1* transgenic mice, four strains showed cardiac expression of the LAMR1-TP1 product.

All four strains expressed LAMR1-TP1 in the heart and were extremely susceptible to RVD (**Fig. 5c**). Sometimes the tissue damage extended to the left ventricle, but right ventricle involvement was always predominant. So far, no phenotypic changes have been detected in the other organs of *Lamr1-tp1* transgenic mice. In contrast, all strains that expressed LAMR1 showed no marked changes in any organ, including the heart. These data indicated that LAMR1-TP1 was responsible for RVD in KK/Rvd mice.

In vitro role of LAMR1-TP1

The *in vitro* expression of LAMR1-TP1 also impaired cardiomyocyte function. Cultured rat cardiomyocytes were transfected with an adenovirus vector containing Lamr1-tp1-IRES-GFP and Lamr1-IRES-GFP under the control of a CA promoter. To clarify the effects of these constructs, we carried out an MTS assay. Only expression of *Lamr1-tp1* by cardiomyocytes led to a decrease of cell numbers 48 h after transfection (**Fig. 6a**), even though the same transfection efficiency was confirmed in all groups based on the level of GFP expression (**Fig. 6b**). On histochemical staining, the most prominent change in these cells was alteration of the chromatin architecture. Staining of heterochromatin by DAPI showed a mosaic pattern in cardiomyocytes transfected with *Lamr1* and a speckled pattern in cardiomyocytes transfected with *Lamr1-tp1*.

We analyzed the localization of LAMR1 and LAMR1-TP1 by confocal microscopy. Rat cardiomyocytes transfected with an adenovirus vector were stained using a LAMR1 antibody (FD4818). This antibody could not distinguish LAMR1 from LAMR1-TP1, but only transfected proteins were stained because endogenous LAMR1 was not detected at its relatively low level of expression. LAMR1 was identified in the DAPI-negative euchromatin area of the nucleus, showing a mirror image to the pattern of DAPI staining (**Fig. 6c**). On the other hand, transfection with *Lamr1-tp1* altered the overall pattern of chromatin as described above and LAMR1-TP1 was partially colocalized with the DAPI-positive heterochromatic loci (**Fig. 6c**). These structural changes to chromatin were observed 10–12 h after transfection and preceded the onset of decreasing cell numbers 24 h after transfection.

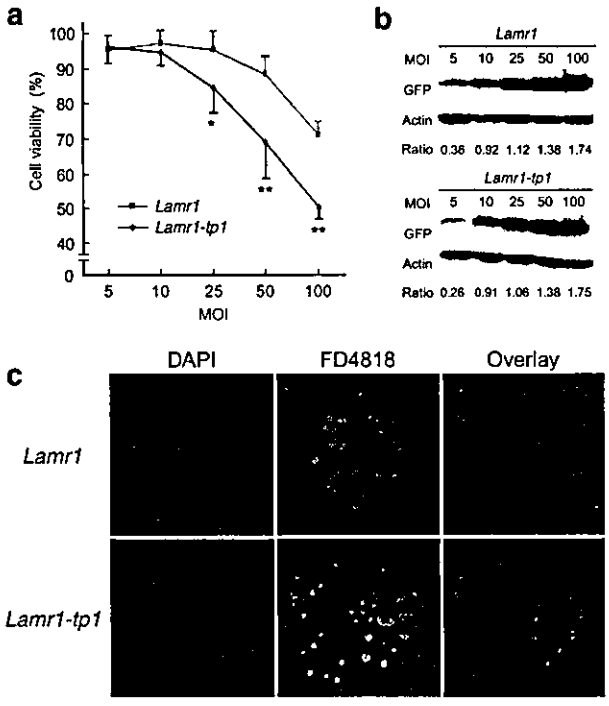

Figure 6 *Lamr1-tp1* caused cardiomyocyte cell death. Cardiomyocytes were infected with recombinant adenoviruses at the indicated multiplicity of infection (MOI). (**a**) Cells expressing *Lamr1-tp1* show lower MTS activity 48 h after adenovirus infection. *$P < 0.05$ versus *Lamr1*; **$P < 0.005$ versus *Lamr1*. (**b**) GFP and actin expression were analyzed 8 h after adenovirus infection. Cell numbers were equivalent at this time point. The ratios of densitometric measurement of GFP:actin are indicated. (**c**) The nuclei of rat cardiomyocytes expressing Lamr1-IRES-GFP or Lamr1-tp1-IRES-GFP were stained with the LAMR1 antibody FD4818 (green) and DAPI (blue). LAMR1 staining showed a perfect mirror image to DAPI-positive area. LAMR1-TP1 was translocated and partially overlapped with DAPI-positive. Scale bar, 20 μm.

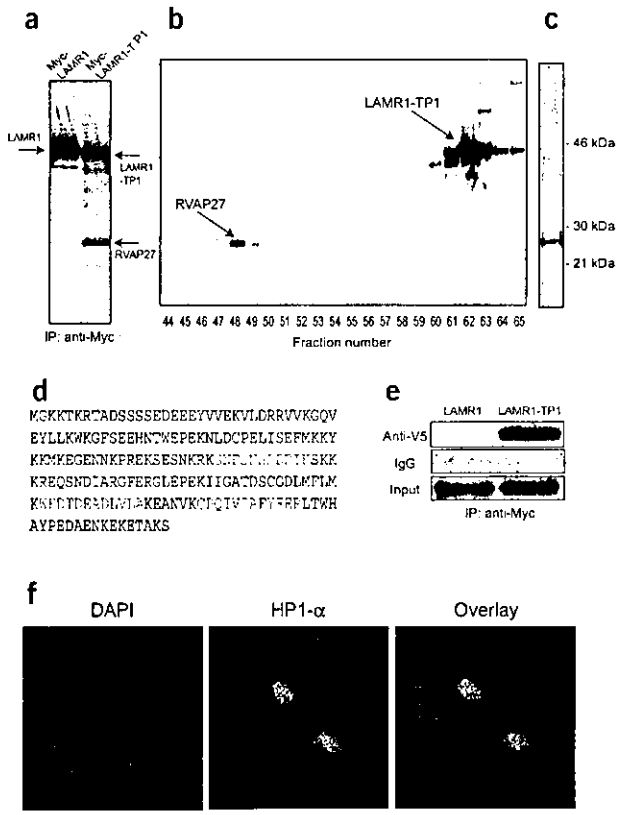

Figure 7 LAMR1-TP1 interacts with HP1-α. (**a**) RVAP27 was immunoprecipitated with LAMR1-TP1 but not with LAMR1 in COS7 cells labeled by ^{35}S-cystein and methionine. (**b**) The complex of radiolabeled LAMR1-TP1 and RVAP27 was separated by a phenyl reverse-phase column. (**c**) The final purification product of RVAP27 was silver-stained. (**d**) The peptides derived from the purified protein, which fitted with those of human HP1-α (as assessed by direct N-terminal sequencing (red) or liquid chromatography-mass spectrometry or mass spectrometry (blue)), are underlined. Cytokine was detected as a Cys-S-propionamide. (**e**) V_5-LAMR1-TP1 but not V_5-LAMR1 expressed in COS7 cells was immunoprecipitated with Myc-tagged HP1-α by anti-Myc. IgG was derived from nonimmunized serum. (**f**) Rat cardiomyocytes were stained with HP1-α antibody, showing HP1-α localization with the DAPI-positive heterochromatin area.

The data suggested that these chromatin changes might have had a lethal effect on the cardiomyocytes, although the possibility that these changes were secondary to lethal cell damage itself cannot be fully excluded.

HP1 binds to mutant LAMR1

To clarify the cellular mechanism by which LAMR1-TP1 caused conformational changes of heterochromatin, we purified and cloned the protein specifically interacting with LAMR1-TP1. The Myc-tagged LAMR1-TP1 fusion protein expressed in ^{35}S-labeled COS7 cells showed the same migration pattern as Myc-tagged LAMR1 (**Fig. 7a**). This 27-kDa protein (named RVAP27) was immunoprecipitated with LAMR1-TP1 but not with LAMR1. Using either a mouse cell line (3T3) or rat cardiomyocytes, we also immunoprecipitated RVAP27 with transfected LAMR1-TP1. Large-scale purification of RVAP27 was done by the sequential use of columns (**Fig. 7b**), and about 10 pmol of RVAP27 was purified from the lysate of 1.0×10^8 COS7 cells (**Fig. 7c**). We analyzed the peptides digested from the RVAP27 band by Edman degradation N-terminal sequencing or nanoelectrospray ionization tandem mass spectrometry. RVAP27 included fragments of the amino acid sequences of SNFSNSADDIK, WKDTDEADLVLA and CPQIVI-AFYEER that matched human heterochromatin protein 1-α (HP1-α) (**Fig. 7d**). The Myc antibody coprecipitated Myc-tagged HP1-α with V_5-tagged LAMR1-TP1, but not with LAMR1; this verified the specific interaction between HP1-α and LAMR1-TP1 (**Fig. 7e**).

HP1 is a key heterochromatin protein that regulates gene silencing by interacting with methylated histones[17]. HP1-α also localizes with DAPI-positive heterochromatin[18]. Cardiomyocytes expressing HP1-α showed the same staining pattern in the DAPI-dense region (**Fig. 7f**). Our immunohistochemical data showed that LAMR1 localized to the euchromatin (DAPI-negative) and that LAMR1-TP1 was partially translocated to heterochromatin (DAPI-positive; **Fig. 6c**). These findings imply that the mutant LAMR1 had an increased affinity for HP1-α and thus was translocated to heterochromatin. Such translocation might influence transcriptional regulation and interfere with the expression of genes essential to the survival of cardiomyocytes, leading to lethal cell dysfunction due to LAMR1-TP1.

Changes of gene expression induced by LAMR1-TP1

To investigate transcriptional regulation by LAMR1-TP1, we analyzed changes in gene expression in cultured cardiomyocytes after transfection of *Lamr1-tp1* or *Lamr1*. Because cells expressing *Lamr1-tp1* began to die 24 h after transfection, we analyzed gene expression at 6 h, 12 h and 24 h (each in duplicate) to exclude the secondary effects of lethal cell damage. GFP expression indicated that the transfected protein was expressed 10 h after transfection, indicating that the expression of genes at 6 h was largely induced by viral infection itself. Transfection with wild-type LAMR1 had a minimal effect on the expression profile compared with that of nontransfected cardiomyocytes, even though the adenovirus vector itself should cause some cell damage (**Supplementary Fig. 1** online). On the other hand, LAMR1-TP1 caused substantial changes in gene expression at 12 h and 24 h, but not at 6 h (**Supplementary Table 1** online). These genes showed similar changes in expression in duplicate analyses. We confirmed further the expression of these genes by quantitative PCR (**Supplementary Fig. 1** online). Our results suggested that LAMR1-TP1, but not LAMR1, could alter the expression of some specific genes. How these genes actually determine the fate of cardiomyocytes needs to be determined in order to understand the pathological role of this mutant protein.

DISCUSSION

Although lethal tachyarrhythmia is often detected in human ARVD, we did not detect it in this mouse model. The difficulty in generating lethal tachyarrhythmia in mice, due to the high beating rate and small size of their hearts[19], might explain our failure to detect lethal arrhythmia. KK/Rvd mice showed electric conduction inhomogeneity leading to prolonged QRS duration, which is often seen in humans with ARVD[20,21]. If similar degradation occurs in the human heart, it will become a focus for lethal arrhythmia at some stage in life. The most important pathological feature of ARVD is the degeneration of right ventricular cardiomyocytes[22]. Our ARVD mouse model reproduced the specific right ventricular degeneration from the outside inwards.

It is still not known why the right ventricle is more susceptible than the left ventricle in these mice. Injection of *Lamr1-tp1* into the left ventricle also induced cardiomyocyte degeneration and calcification,